CASL-U-2015-0134-000

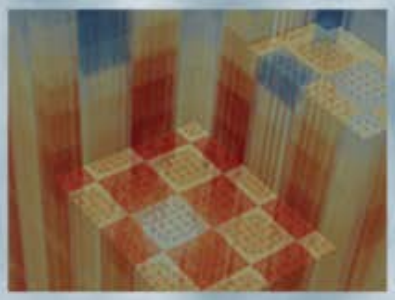

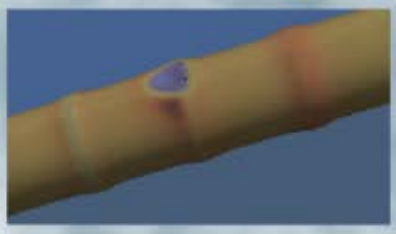

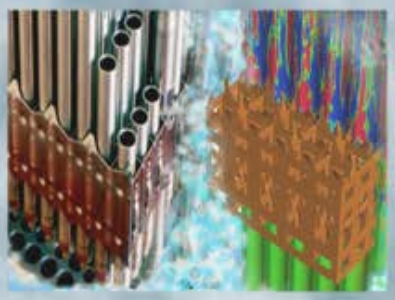

MPACT Verification and Validation: Status and Plans

Tom Downar Brendan Kochunas
Univ of Michigan

Ben Collins
Oak Ridge National Laboratory

April 30, 2015

REVISION LOG

Revision	Date	Affected Pages	Revision Description
0		All	Initial Release

Document pages that are:

Export Controlled _____None_____

IP/Proprietary/NDA Controlled____None_____

Sensitive Controlled_____None_____

Requested Distribution:

To:

Copy: SLT

EXECUTIVE SUMMARY

The MPACT code provides the capability to calculate the steady-state reactor core neutron distribution for operating nuclear power plant (PWR) conditions across multiple fuel cycles. This document provides an initial plan and summarizes the current status of the verification and validation (V&V) of MPACT. The V&V described here is one step in the overall software life cycle as described in the CASL Software Quality Assurance plan [Seiger, 2015], and provides the primary means of building confidence and credibility in the ability of MPACT to simulate the neutronics behavior of a nuclear reactor. Within the context of SQA activities, verification and validation (V&V) is generally the largest area of work with verification providing evidence that the computational model is solved correctly and accurately, and validation providing evidence that the mathematical model accurately relates to experimental measurements. As required in the CASL SQA plan, it is the responsibility of UM and ORNL as owners of MPACT to ensure that verification and validation activities are performed and documented in a V&V manual with supporting publications and CASL technical reports which can be distributed for reference and distribution within VERA. The objective of this document is to summarize the current state of MPACT V&V and establish the framework for future MPACT V&V activities.

During Phase I of CASL, MPACT verification activities in the areas of source code verification have matured and a plan has been established to provide a more robust solution verification effort based on the Method of Manufactured Solutions. Several specific tasks were identified to improve MPACT verification during Phase II of CASL, to include a task to improve the unit and regression test coverage in MPACT, a task to develop a plan to document all of the unit and regression tests in a consistent format that can be assimilated into a common document, and a joint UM/ORNL task to develop standardize coding standards and workflow for the continued collaborative development of MPACT.

During Phase I of CASL, MPACT validation work has been ongoing in both the areas of measured data from critical experiments as well as measured data from operating nuclear power plants. Both of these areas have been supplemented with calculated quantities on fine scales from continuous energy (CE) Monte Carlo methods. Based on the results of Phase I V&V, the confidence level has increased in the ability of MPACT to model an operational Pressurized Water Reactor. A roadmap has been established by the VERA-CS Validation Plan [Godfrey, 2014] to guide the efforts during Phase II and to further increase the validation base of the code. Areas were identified which require increased emphasis during Phase II such as validation of MPACT depletion with measured isotopics, implementation of a formal data uncertainty quantification (UQ) protocol in MPACT, the addition of problems to validate the pin resolved capability in MPACT, and a coordinated effort with VMA to insure that the validation needs identified by the PCCM on the CASL challenge problems are covered sufficiently by the MPACT validation suite.

CONTENTS

EXECUTIVE SUMMARY **iii**

CONTENTS **iv**

FIGURES **v**

ACRONYMS **vii**

1. Introduction **1**

2 Verification **2**

2.1 Source Code Verification 2

2.1.1 Unit Testing 2

2.1.2 Regression Testing 6

2.2 Solution Verification 10

2.2.1 Mesh Convergence Analysis 10

2.2.2 Method of Manufactured Solutions 12

3 Validation **17**

3.1 Background 17

3.2 Validation Activities in MPACT During CASL Phase I 20

3.2.1 Critical Experiments 20

3.2.1.1 Babcock & Wilcox Critical Experiments 21

3.2.2.2 The Special Power Excursion Reactor Test (SPERT) 28

3.2.2 Operating Power Plants 37

3.2.2.1 Watts Bar Nuclear Plant 37

3.2.2.2 BEAVRS 41

3.2.2.3 KRSKO 41

3.3 Post Irradiation Examination / Depletion 42

3.4 Continuous Energy Monte Carlo Benchmarks 42

4 Summary, Conclusions, Future Work **43**

References **46**

FIGURES

Figure 1. Unit Test Problem Description 3
Figure 2. Regression Test Problem: 3 x 3 pin cell 8
Figure 3. Regression Test Problem Solution 8
Figure 4. MPACT Regression Suite Matrix [Collins, 2015] 9
Figure 5. VERA Benchmark Problems for Mesh Convergence Study (Pin Cell and Assembly) 10
Figure 6. Spatial grid of 1D slab (optical thickness, in units of mean-free-path) 13
Figure 7. Angular flux (L), Numerical solutions from various implementations (R) 15
Figure 8. Four Components of VERA-CS Validation [Godfrey, 2014] 18
Figure 9. VERA-CS Validation Assessment Matrix [Godfrey, 2014] 19
Figure 10. B&W Critical Experiment Facility 21
Figure 11. B&W-1484 Core 4:1 (Top) Core 4:2 (Bottom) 22
Figure 12. B&W-1810 Core 8:1 Layout 25
Figure 13. B&W-1810 Core 8:1 Fission Rate Difference, Center Assembly 27
Figure 14. B&W-1810 Core 8:5 Fission Rate Difference, Center Assembly 27
Figure 15. B&W-1810 Core 8:12 Fission Rate Difference, Center Assembly 27
Figure 16. SPERT III E-core cross-section. 29
Figure 17. MPACT 25-rod Fuel Assembly Model 30
Figure 18. MPACT model for core filler 30
Figure 19. MPACT model for axial grids 31
Figure 20. MPACT model for flux suppressors 31
Figure 21. MPACT model for middle of active core 32
Figure 22. Comparison of control rod worth for CZP 33
Figure 23. Comparison of fission rate distribution– CZP 34
Figure 24. Comparison of fission rate distribution– HZP 34
Figure 25. Comparison of pin-wise fission rates of the peak power assemblies 35
Figure 26. Axial fission rates distribution 36
Figure 27: VERA Problem 5 Assembly, Poison, and Control Rod Layout in Quarter Symmetry 37
Figure 28: Problem 10 WBN1 Cycle 2 Core Loading Pattern 38
Figure 29: Core Power Distribution at BOC HZP (Left) and BOC HFP (Right) 40
Figure 30: Comparison of Cycle 1 Critical Boron 41
Figure 31: Westinghouse Optima2 Fuel Assembly Used for Pin Measurements [Macku, 2007] 44

TABLES

Table 1. MPACT Code Testing Statistics 5
Table 2. Sensitivity Study for VERA Benchmark Problem 1a (Regular Pincell) 11
Table 3. Sensitivity Study for VERA Benchmark Problem 2a (Regular Assembly) 12
Table 4. Convergence Study (LHS) and Summary of Error (RHS) for the MMS Example 15
Table 5. Sample PHI KANBAN Ticket Tracking Validation Activities in MPACT 20
Table 6. Summary of Geometric Buckling & Critical Height Values 23
Table 7. B&W-1484 Core 4:1 and 4:2 MPACT-Calculated Eigenvalues 23
Table 8. B&W-1810 Benchmark Configuration Summary 25
Table 9. B&W-1810 Benchmark Results 26
Table 10. Basic Core / Fuel Data for SPERT III E-core 29
Table 11. Comparison of eigenvalues 33
Table 12. Comparison of critical control rod position 33
Table 13: Cycle 1 Simulated Operating History 38
Table 14: Measured and Simulated Cycle 1 States 40

ACRONYMS

CASL Consortium for Advanced Simulation of Light Water Reactors
CP Challenge Problem
CRUD corrosion-related unidentified deposits or Chalk River unidentified deposits
CTF COBRA-TF subchannel thermal-hydraulics code
DOE US Department of Energy
EPRI Electric Power Research Institute
FA Focus Area
HZP Hot Zero Power
LANL Los Alamos National Laboratory
LWR light water reactor
MOC method of characteristics
OLCF Oak Ridge Leadership Computing Facility
OR operational reactor
ORNL Oak Ridge National Laboratory
PCI pellet-cladding interaction
PCM percent mille (10-5)
PHI Physics Integration
PoR plan of record
PWR pressurized water reactor
QOI quantity of interest
RSICC Radiation Safety Information Computational Center
RTM Radiation Transport Methods
SA sensitivity analysis
SNL Sandia National Laboratories
T/H thermal-hydraulics
THM Thermal Hydraulics Methods
UQ uncertainty quantification
UM University of Michigan
V&V verification and validation
VERA Virtual Environment for Reactor Applications
VMA Validation and Modeling Applications
VR virtual reactor
VRI Virtual Reactor Integration Focus Area
VUQ Validation and Uncertainty Quantification
VVUQ Verification, Validation and Uncertainty Quantification
WEC Westinghouse Electric Company

1. INTRODUCTION

This document provides an initial plan and summarizes the current status of the verification and validation (V&V) of the reactor neutronics code MPACT. The V&V described here is one step in the overall software life cycle as described in the CASL Software Quality Assurance plan [Seiger, 2015], and provides the primary means of building confidence and credibility in the ability of MPACT to simulate the neutronics behavior of a nuclear reactor. Within the context of SQA activities, verification and validation (V&V) is generally the largest area of work with verification providing evidence that the computational model is solved correctly and accurately, and validation providing evidence that the mathematical model accurately relates to experimental measurements. As required in the CASL SQA plan, it is the responsibility of UM and ORNL as owners of MPACT to ensure that verification and validation activities are performed and documented in a V&V manual with supporting publications and CASL technical reports which can be distributed for reference and distribution within VERA. The objective of this document is to summarize the current state of MPACT V&V and establish the framework for future MPACT V&V activities. The following sections will provide an overview of the verification and validation process in MPACT, and a summary of the status of each component of V&V in the code.

2 VERIFICATION

The overarching objective of code verification is to establish that a model implemented in the code accurately represents the developer's conceptual description and the solution of the model. The verification activities in MPACT have been designed to address this general objective and encompass both the verification of the source code itself as well as the verification of the solution. Source code verification activities in MPACT have been directed toward identifying mistakes in the source code itself by establishing comprehensive software testing practices, whereas the solution verification activities within MPACT have been directed toward evaluating the numerical error in the solution itself. The following section will first address the source code verification and summarize the current status of the source code verification activities. The subsequent section will then describe the solution verification activities currently in progress and those planned for the code.

2.1 Source Code Verification

The two principal components of source code verification in MPACT are unit testing and regression testing. Unit testing is a software testing method by which individual units of source code are tested to determine whether they are fit for use. In contrast, regression testing seeks to uncover new software bugs or *regressions*, in existing functional and non-functional areas of the code after changes have been made to the source. The following subsections will describe unit testing and regression testing practices in MPACT.

2.1.1 Unit Testing

The overall goal of unit testing is to isolate each part of the program and show that the individual parts are correct. The testing in MPACT was designed to verify the smallest testable part of an application and each test case was designed to be independent from the others. The practice in MPACT has been for developers to create unit tests for all functions and methods while the code itself is being written. When the tests pass, that phase of the code development is considered complete. However, if a unit test fails, there is considered to be a bug either in the changed code or the tests themselves, and that phase of the code development process is continued. The unit tests accelerate the process of correcting the bug by allowing the location of the fault or failure to be easily traced [Kolowa, 2007].

During MPACT development, unit testing has served the important role of finding problems early in the development cycle. All unit testing in MPACT is run repeatedly as the larger code base is developed via an automated process. This has simplified the process of locating a fault or failure since the unit tests have alerted the development team of the problem before the code is handed off to testers or users.

One of the challenges in writing the unit tests within MPACT has been the difficulty of setting up realistic tests with relevant initial conditions so the part of the application being tested behaves like part of the complete system. If these initial conditions are not set correctly, the test will not be exercising the code in a realistic context, which diminishes the value and accuracy of unit test results. This can best be illustrated with the following unit test example which is currently used in MPACT.

MPACT Unit Test Example

One of the principal unit tests implemented in the MPACT code is the solution of the mono-energetic flux for a purely absorbing 1-D homogeneous medium with fixed boundary conditions. The test problem shown in Figure **1** is a square medium with 4x4 modules and 2x2 pins. Each pin itself has a mesh of 4x4 and the modules are 2x2 cm nodes which makes problem domain 8x8cm square. The north and south surfaces have a reflective boundary while the west and east surfaces are a vacuum.

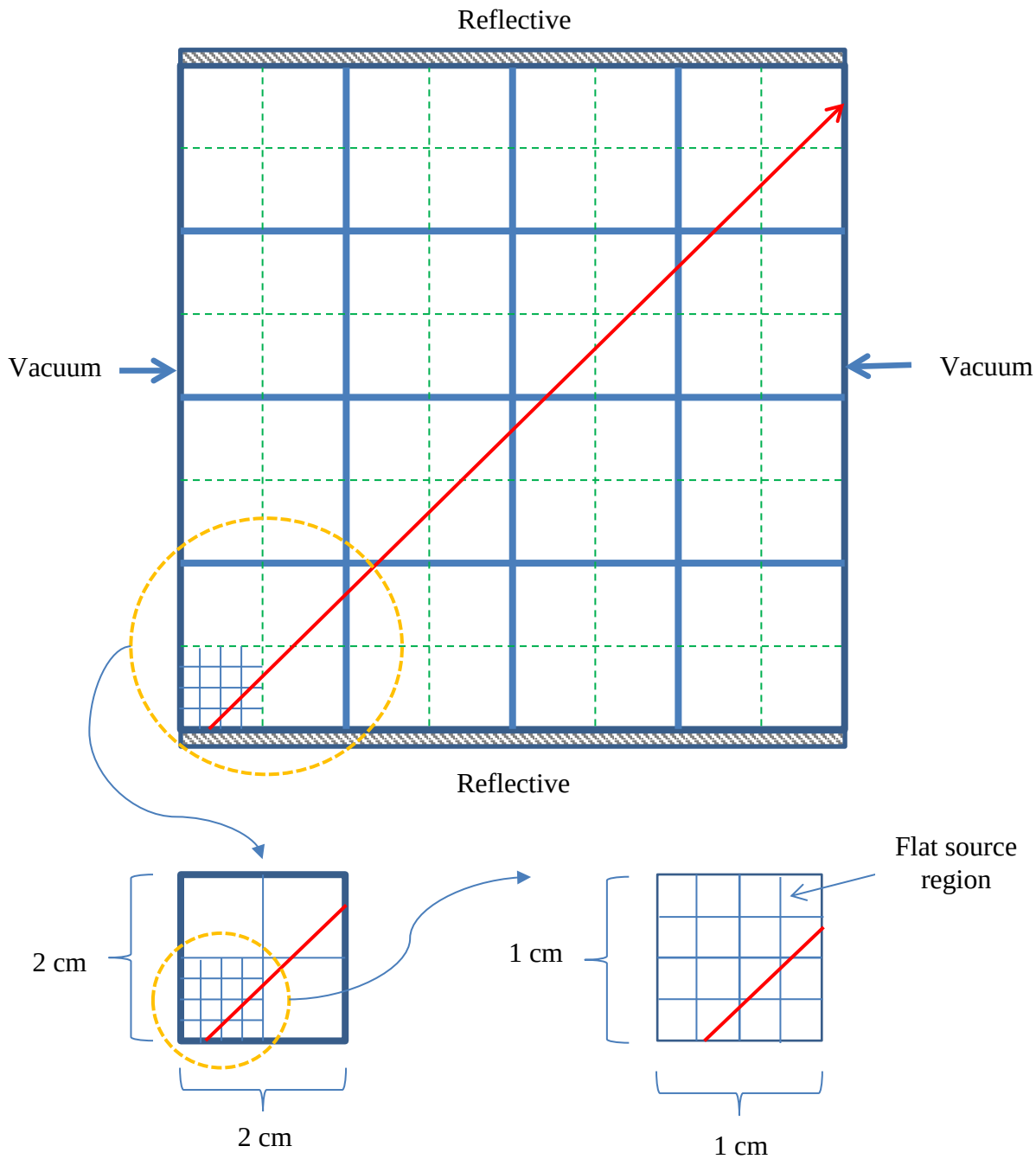

Figure 1. Unit Test Problem Description

The boundary angular surface flux is set to a fixed value (which is 2 for this test) on the west side of the rays. The external source is set to zero which results in the analytical solution given in Eq (1) which is loaded into a specific variable in the code from an external file.

$$\psi^{out} = \psi^{in} e^{-\Sigma_t s} \qquad (1)$$

The focus of this unit test is the Product Quadrature sweeper module of the MOC solver in the code which loops through angles in the azimuthal quadrature set which is the "Chebyshev" quadrature for this problem. For each angle in the azimuthal quadrature set the long rays are swept and modular rays are looped through for each long ray. For each modular ray the angles are swept in the polar quadrature set which is the Gauss quadrature for this problem.

The code fragment for the unit test is given below. Similar testing is repeated for different type of boundary condition applied to different surfaces.

```
!Test sweep for mono-energetic with fixed boundary in purely absorbing 1-D homogeneous media
!Test all faces

!
!West face, Mono-Directional
!Standard Sweep

      COMPONENT_TEST('sweep(1,3,0.0_SRK) (Mono-Directional)')

      !Clear volumetric source
      testSource%qext=0.0_SRK
      CALL testMOCSweeperType%setExtSource(testSource)

      !Set boundary source on west face and make it mono-directional
      CALL readRef2dSolution(1)
      CALL testMOCSweeperType%setFluxVal(0.0_SRK)
      DO iang=1,1
        DO i=1,UBOUND(testMOCSweeperType%phiang(1)%angle(iang)%face(1)%angflux,DIM=2)
          testMOCSweeperType%phiang(1)%angle(iang)%face(1)%angflux(:,i)=2.0_SRK
        ENDDO
      ENDDO
      testMOCSweeperType%longRayDat%bcType=PERIODICBC
      testMOCSweeperType%longRayDat%bcType(1)=VACUUMBC
      testMOCSweeperType%longRayDat%bcType(3)=VACUUMBC
      testMOCSweeperType%updateBC%bcType(1:4)=testMOCSweeperType%longRayDat%bcType

      CALL testMOCSweeperType%sweep(1,3,0.0_SRK) !Sweep

      !Test scalar flux
      bool=ALL(ref2dsol*PI .APPROXEQ. testMOCSweeperType%phis(:,1))
      ASSERT(bool,'testMOCSweeperType%sweep(1,3,0.0_SRK) (Mono-Directional)')
```

MPACT Unit Testing Statistics

Within MPACT unit testing has provided a living documentation of the overall code system. Below is a summary table of the current code statistics with some footnotes.

Table 1. MPACT Code Testing Statistics*

Metric	M_libs	M_Drivers	Total
Unit Tests	123	4	127
Regression Tests	0	159	159
Coverage	80.17%	67.24%	79.69%
Lines of Code	91,006	3,446	94,452
Automated Testing			
Continuous[1]	Yes	Yes	
Nightly[2]	Yes	Yes	
Portability[3]	Yes	Yes	
Verification[4]	Yes	Yes	
Validation[5]	No	Yes	
Memory[6]	Yes	Yes	
Coverage[7]	Yes	Yes	

*Data as of 4/30/15

1 - Test Server checks for changes every 10 minutes and tests two configurations
2 - Tests many more regression tests, performed by CASL and UM test machines
3 - Test GCC 4.6.1, 4.7.2, 4.8.1, Intel 12.1.5 with and without MPI & other TPLs
4 - Unit tests for solver kernels test against analytic solutions. Some regression tests compare against analytic solutions.
5 - Depletion solver is compared to experimental results.
6 - This means analyzing program with Valgrind
7 - This means running "gcov" on all tests.

Since unit testing only tests the functionality of the units themselves, it is recognized that unit testing will not catch every error in the program. Specifically, unit testing does not catch integration errors or broader system-level errors (such as functions performed across multiple units, or non-functional test areas such as performance). Therefore in MPACT unit testing is performed in conjunction with regression testing which will be described in the next section.

2.1.2 Regression Testing

The primary objective of regression testing is to provide a series of functional tests that can be repeatedly performed during code development so that the code output can be compared against previously recorded outputs to ensure that new features and enhancements do not alter the reproducibility of existing features. Regression testing has served the important role during MPACT development to ensure that changes in one part of the code do not introduce new faults in other parts of the code.

As described in the previous section, unit tests were designed in MPACT to exercise individual functions or subroutines, whereas regression tests are more comprehensive and are designed to provide functional tests which exercise significant sections of the program with various inputs. The MPACT regression testing targets key features that the user will need when applying the code to practical LWR problems. A summary of some of the key capabilities tested include:

- **Geometry**
  - Cylindrical, Quarter, Rectangular and Generalize cylinder pin geometries
  - Inserts
  - Control rod (+ rod movement)
  - Baffle/Reflector
  - Upper/lower nozzle, core plate, reflector
  - Multiple assemblies/modules
  - Symmetry
  - Grids
  - detectors

- **Transport Solvers**
  - P0 and Pn 2D MOC
  - P0 and Pn 2D-1D with SP3 (and NEM)

- **Other solvers**
  - Depletion (native and Origen)
  - Search (boron, rod)
  - Multistate
  - CMFD (Multilevel, MGNode, 1Gsweep)
  - Feedback (internal and CTF)
  - Eq Xe/Sm
  - XS Shielding (Subgroup vs ESSM)
  - Cusping treatment

- **Parallel**
  - MPI (space, angle, space+angle), explicit file
  - OpenMP (threading)

In addition, new regression tests in MPACT are sometimes added as part of the process of performing software fixes to the code. Experience has shown that old faults can re-emerge since at times a fix for a problem in one area has inadvertently caused a software bug in another area. Or when some feature was redesigned, some of the same mistakes that were made in the original implementation of the feature were made in the redesign. The best practice used in MPACT is that when a bug is located and fixed, a test is recorded that exposes the bug and the test is rerun regularly after subsequent changes to the program. Both the unit and regression testing are used to rerun previously completed tests to determine whether previously fixed faults have re-emerged. The MPACT developer can also systematically select the appropriate minimum set of tests needed to adequately cover a particular change.

Current practice in MPACT is to document all unit and regression testing with comments in the source code. However, consistent with the CASL SQA requirements, the plan is for all MPACT tests to be documented and configuration-controlled with the following information:

1. The author or owner of the test;
2. The purpose of the test, including whether the test is a regression test, verification test, performance test, etc.;
3. The requirement or feature being tested; and
4. The pass/fail criteria for the test.

The regression tests in MPACT are also implemented as a scripted series of program inputs with a driver layer that links to the code without altering the code being tested. An automated system is in place to re-run all regression tests nightly and a report is prepared of any failures. These tests are compared to previous solutions from MPACT to ensure consistent answers. The acceptance criteria for regression test problems in MPACT is currently set to be ±10 pcm for k-effective and a 0.5% maximum change in pin powers and ±1 ppm for the boron concentration.

Sample MPACT Regression Test Problem

The essential features of a regression test problem can be demonstrated by one of the current regression tests in MPACT. One of the continuously run regression tests in MPACT is a 3 by 3 pin cell problem as shown in Figure 2. The pin-cells are stacked 2 nodes tall with the radial pin pitch of 1.26 cm and the axial node height of 5cm. The central location of the 3 by 3 array is occupied by a guide tube while the other cells are fuel pins. The pins are composed of fuel, helium gap and zirconium cladding and the guide tube is zirconium as well.

All the boundaries in the problem are reflective and the Chebyshev-Yamamoto quadrature set is used with 1 polar and 8 azimuthal octants. A ray spacing of 0.08 cm is used with flux tolerance of 1e-4 and eigenvalue tolerance of 1e-4. The problem is performed with a 60 group library set with 4 subgroups for the resonance self-shielding. The solution for this problem is stored for comparison with the expected k-effective of 1.17933 and pin powers as shown in Figure 3.

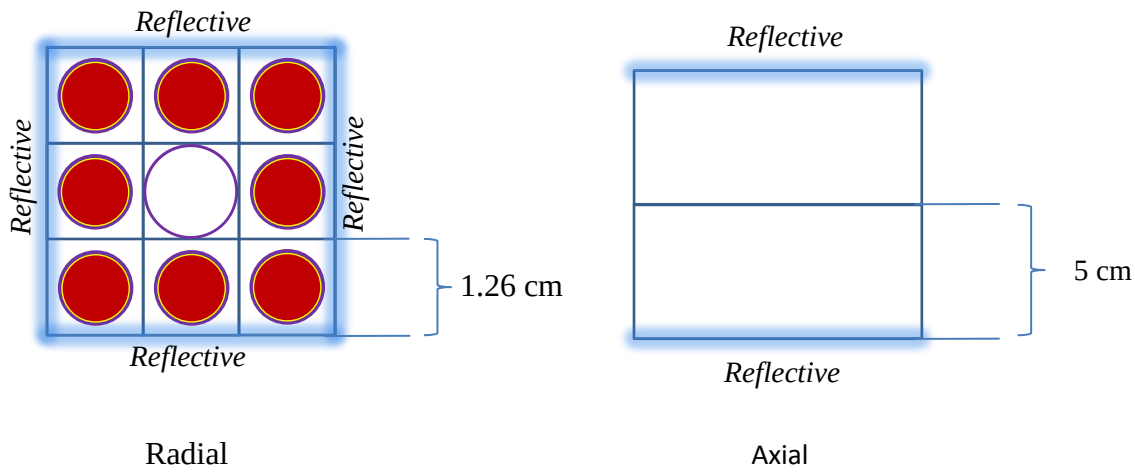

Figure 2. Regression Test Problem: 3 x 3 pin cell

0.99180	1.00820	0.99180
1.00820	0.00000	1.00820
0.99180	1.00820	0.99180

Figure 3. Regression Test Problem Solution

Design of Regression Test Suite

As part of the regression test plan for MPACT, a comprehensive regression test matrix is being developed and will be provided as part of a CASL report [Collins, 2015]. The test matrix from that plan is shown in Figure 4 and will provide the roadmap for the development of regression testing in MPACT.

		Geometry													Solvers																			Sym		Parallel						
		Quarter	Full	Assembly Gap	Nozzles	Core Plates	Reflector	Baffle	Inserts	Control Rods	Detector	Nominal Spacers	Above/below fuel	IFM	Explicit	2D P0	2D Pn	2D/1D NEM	2D/1D SP3	CMFD 1g	CMFD MG	Search keff	Search boron	Search rod	Multistate	Depletion native	Depletion origen	Shuffle rotational	Shuffle mirror	InternalTH	CTF	Eq Xe/Sm	Subgroup	ESSM	Cusping	Mirror	Rotational	Space ztree	Space explicit	Angle	Thread	Space+angle	Angle + thread	Space + angle + thread
Geometry	Quarter			X	X	X	X	X	X	X	X	X	X	X	X	X	X			X		X			X	X	X	X	X	X	X	X	X	X	X	X	X	X	X	X	X	X	X	X
	Full			X	X	X	X	X	X	X	X	X	X	X	X	X	X				X	X								X	X							X	X					
	Assembly Gap				X	X	X									X					X									X	X													
	Nozzles					X	X																																					
	Core Plates						X																																					
	Reflector																																											
	Baffle																																											
	Inserts										X																																	
	Control Rods										X																																	
	Detector																								X											X	X	X						
	Nominal Spacers																	X	X																									
	Above/below fuel																	X	X																									
	IFM																	X	X																									
	Explicit															X	X													X	X													
Solvers	2D P0																	X	X							X	X					X	X	X		X	X	X	X	X	X	X	X
	2D Pn																	X	X							X	X					X	X	X		X	X	X		X	X		X
	2D/1D NEM																																X	X		X	X	X	X		X		
	2D/1D SP3																																X	X		x	X	X	X	X		X		
	CMFD 1g																																			X	X	X	X	X		X		
	CMFD MG																																			X	X	X	X	X		X		
	Search keff																								X					X	X	X												
	Search boron																								X					X	X	X												
	Search rod																								X					X	X	X	X	X	X									
	Multistate																																											
	Depletion native																											X	X			X						X	X					
	Depletion origen																											X	X			X						X	X					
	Shuffle rotational																																			X	X	X	X			X		
	Shuffle mirror																																			X	X	X	X			X		
	InternalTH																																X	X				X	X	X		X		
	CTF																																X	X		X	X	X	X	X		X		
	Eq Xe/Sm																																					X	X	X		X		
	Subgroup																																			X	X	X	X	X		X		
	ESSM																																			X	X	X	X	X		X		
	Cusping																																											
Sym	Mirror																																					X	X	X	X	X	X	X
	Rotational																																					X	X	X	X	X	X	X
Parallel	Space ztree																																											
	Space explicit																																											
	Angle																																											
	Thread																																											
	Space+angle																																											
	Angle + thread																																											
	Space + angle + thread																																											

Figure 4. MPACT Regression Suite Matrix [Collins, 2015]

2.2 Solution Verification

The principal focus of solution verification activities within MPACT has been to evaluate the numerical error in the solution. The initial focus of solution verification was to perform mesh convergence analysis in support of the initial code validation activities in MPACT [Wang, 2014]. However a more comprehensive and thorough solution verification has been planned based on the Method of Manufactured Solutions (MMS). The following section will first summarize the initial mesh convergence analysis and the subsequent section will describe the planned MMS work.

2.2.1 Mesh Convergence Analysis

The Method of Characteristics (MOC) is one of the essential solution algorithms in MPACT. However, the MOC solver is a nonstandard discretization method and the solution sensitivity to the various discretization parameters is not yet well understood. A better understanding of mesh convergence is also an essential first step in applying Method of Manufactured Solution. The work used the various VERA benchmark cases to evaluate the sensitivity of k-eff to the MOC parameters for selected VERA benchmark cases. The difference between keff for the specific case and keff for the most highly resolved case was used as the metric of performance. The MOC parameters varied included the flat source region (FSR) mesh (the number of radial and azimuthal discretization), the order of the quadrature set (the number of azimuthal angles), and the ray spacing. The selected VERA benchmark cases covered pin cell problems (left) and assembly problems (right) as shown in Figure 5.

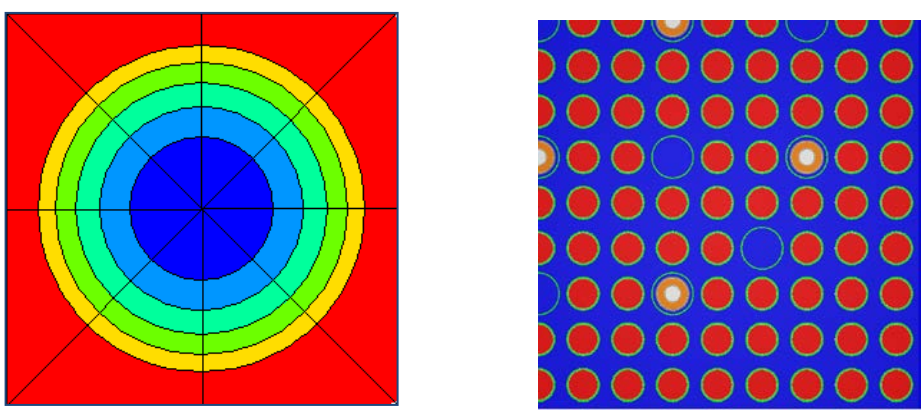

Figure 5. VERA Benchmark Problems for Mesh Convergence Study (Pin Cell and Assembly)

The detailed results are provided in [Wang, 2014] but the selected conclusions from the sensitivity studies are given in the Table 2 and Table 3 below and some of the findings are summarized as follows:

1. For all cases, the sensitivity of keff to the FSR mesh is low as long as long as the FSR mesh is not too coarse and the ray spacing resolves the smallest region (i.e., the IFBA coating). The conclusion is that given a sufficiently fine ray spacing, 3 radial rings in the fuel, 2 radial rings in the moderator, and 8 slices for azimuthal discretization will provide sufficient accuracy.

2. For all cases, the sensitivity of the results to the quadrature set is moderate and a reasonable set is 16 azimuthal angles per quadrant and 3 polar angles per hemisphere.

3. The sensitivity of keff to the ray spacing is strong and the ray spacing needs to be comparable to the thickness of the smallest region, such as an IFBA coating.

4. There are nonlinear relationships among the MOC parameters and their impact on keff and this makes it difficult to determine an optimum set of MOC parameters that will hold for all cases, especially when taking into account computational time. For example, the FSR mesh is not a continuously changing variable and keff oscillates with the ray spacing and the number of azimuthal angles, which means that the change in keff due to a change in either of these quantities is a function of the other variable.

5. Overall, sensitivities of keff to the FSR mesh, angular quadrature, and ray spacing are mitigated in problems with a larger computational domain. However, large problems involving very thin regions shows stronger sensitivity to MOC parameters than those without very thin region

Table 2. Sensitivity Study for VERA Benchmark Problem 1a (Regular Pincell)

MOC Parameter	**Sensitivity**	**Observations**
FSR mesh	Slight	Adequate accuracy is obtained as long as the FSR mesh is not too coarse - 3 rings in fuel and 2 rings in moderator for radial discretization and 8 slices for azimuthal discretization are suggested.
Angular quadrature	Moderate	k-diff changes drastically when quadrature set order is changed - 16 azimuthal angles in (0, PI/2) and 3 polar angles in (0, PI/2) are suggested.
Ray spacing	High	k-diff oscillates with dray, but after dray decreases to 0.01 cm, the amplitude of oscillation is bounded within ±50 pcm range, so 0.01 cm is suggested

Table 3. Sensitivity Study for VERA Benchmark Problem 2a (Regular Assembly)

MOC Parameter	Sensitivity	Observations
FSR mesh	Slight	k-diff is only slightly sensitive to FSR mesh, adequate accuracy is obtained as long as the FSR mesh is not too coarse - 3 rings in fuel and 2 rings in moderator for radial discretization and 8 slices for azimuthal are suggested.
Angular quadrature	Moderate	k-diff is still sensitive to the quadrature set order, although to a smaller extent. Order 16 and 3 is suggested, after which the amplitude of oscillation is bounded and going to higher order up to 32 only gives at most another 50 pcm accuracy.
Ray spacing	High	k-diff is much less sensitive to ray spacing – the maximum accuracy gained by reducing dray from 0.08 to 0.005 cm is only 35.2 pcm in this input space, average accuracy gain being 16.8 pcm. So for a problem that does not involve very thin regions, ray spacing as large as 0.08 cm or even larger is acceptable.

2.2.2 Method of Manufactured Solutions

A simple mesh convergence analysis has several limitations and it would be more robust to use the error between successively refined numerical solutions and the exact analytic solutions as the metric to achieve solution verification. However, exact analytical solutions are generally only possible for a very limited set of problems. A more flexible technique is being investigated for implementation in MPACT based on the Method of Manufactured Solution (MMS), which requires that the analytically derived source term be inserted into the code being tested. As discussed in [Oberkampf, 2008], the MMS is capable of verifying several numerical aspects in the code, such as the mathematical correctness of the numerical algorithms, the grid-spacing technique, and the absence of coding errors in the software implementation. MMS has been used successfully with other transport codes [Pautz, 2001] and this section will first provide a simple example developed as part of investigating MMS for MPACT [Wang, 2015] and then discuss preliminary plans to apply MMS in MPACT.

The essential idea of MMS is instead of solving a specified problem with prescribed boundary and initial conditions, one can specify the solution (Manufactured Solution) beforehand and substitute the solution into the equation which the solver claims to have solved. This results in an extra

analytical source (Manufactured Source). It is this source that would produce the solution that one started with. The boundary and initial conditions can be obtained by evaluating the manufactured solution at the boundary and at initial time. This set of boundary and initial conditions, together with the manufactured source have "manufactured" a problem from which the exact analytical solution is already known. By comparing the numerical solution from the solver with the manufactured analytical solution and observing the expected rate of convergence in the successive refinements, the numerical code can be verified. This process can be demonstrated with the following example.

MMS Example Problem

A mono-energetic fixed source problem in a homogenous one dimensional slab can be written as:

$$\begin{aligned} &\mu\frac{\partial\psi}{\partial\tau}(z,\mu)+\Sigma_t\psi(z,\mu)=\frac{\Sigma_s}{2}\int_{-1}^{1}\psi(z,\mu')\,d\mu'+\frac{Q(z)}{2} \\ &\psi(0,\mu)=\psi^b\,,\quad 0\le\mu\le 1, \\ &\psi(\mathrm{T},\mu)=0\,,\quad -1\le\mu\le 0. \end{aligned} \tag{2}$$

Dividing both sides by Σ_t, Eq. (2) is transformed in the following form where spatial variables are in units of mean free path, c being the scattering ratio.

$$\begin{aligned} &\mu\frac{\partial\psi}{\partial\tau}(\tau,\mu)+\psi(\tau,\mu)=\frac{c}{2}\int_{-1}^{1}\psi(\tau,\mu')\,d\mu'+\frac{Q(\tau)}{2} \\ &\psi(0,\mu)=\psi^b\,,\quad 0\le\mu\le 1, \\ &\psi(\mathrm{T},\mu)=0\,,\quad -1\le\mu\le 0. \end{aligned} \tag{3}$$

For this example, the Discrete Ordinates (Sn method) can be used to treat the angular dependence with n=32, and auxiliary equations can be formed with the diamond difference scheme (with alpha set as zeros) on the following spatial grid (

Figure 6).

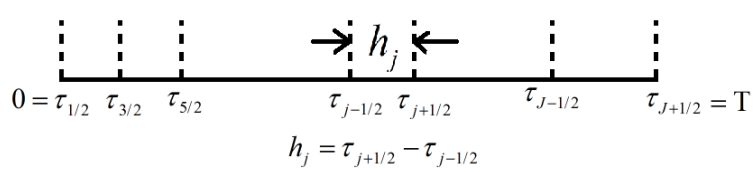

Figure 6. Spatial grid of 1D slab (optical thickness, in units of mean-free-path)

$$\frac{\mu_n}{h_j}\left(\psi_{n,j+\frac{1}{2}}-\psi_{n,j-\frac{1}{2}}\right)+\psi_{n,j}=\frac{c}{2}\sum_{m=1}^{N}\psi_{m,j}w_m+\frac{1}{2}Q_j\,,\quad 1\le n\le N, 1\le j\le J$$

$$\psi_{n,j}=\frac{1+\alpha_{n,j}}{2}\psi_{n,j+\frac{1}{2}}-\frac{1-\alpha_{n,j}}{2}\psi_{n,j-\frac{1}{2}}\,,\quad 1\le n\le N, 1\le j\le J \tag{4}$$

$$\psi_{n,\frac{1}{2}}=\psi_n^b\,,\quad \frac{N}{2}+1\le n\le N,\left(\mu_n>0\right)$$

$$\psi_{n,J+\frac{1}{2}}=0\,,\quad 1\le n\le\frac{N}{2},\left(\mu_n<0\right)$$

A manufactured solution can be assumed: $\psi=\psi_0+\psi_1\tau^2e^{\mu}$ (The selection can be arbitrary, and this choice is to ensure both spatial and angle dependences. Using this in Eq.(3) provides the following manufactured source.

$$Q\left(\tau,\mu\right)=\psi_2\cdot\mu e^{\mu}\cdot 2\tau+\psi_0+\psi_2\cdot\tau^2e^{\mu}-\frac{c}{2}\left[2\psi_0+\psi_2\cdot\tau^2\left(e-e^{-1}\right)\right] \tag{5}$$

Which can then be averaged over a spatial cell $\left(\tau_{j-\frac{1}{2}},\tau_{j+\frac{1}{2}}\right)$ to give:

$$\begin{aligned}Q_{n,j}&=\psi_2\cdot\mu e^{\mu}\cdot\left(\tau_{j-\frac{1}{2}}+\tau_{j+\frac{1}{2}}\right)+\left(1-c\right)\psi_0\\&+\psi_2\cdot\left[e^{\mu}-\frac{c}{2}\left(e-e^{-1}\right)\right]\cdot\frac{1}{3}\cdot\left[\tau^2_{j-\frac{1}{2}}+\tau^2_{j+\frac{1}{2}}+\tau_{j-\frac{1}{2}}\tau_{j+\frac{1}{2}}\right]\end{aligned} \tag{6}$$

Evaluating the manufactured solution at the left and right edges of the slab gives,

$$\begin{aligned}&\psi_{n,\frac{1}{2}}=\psi_0\,,\quad \frac{N}{2}+1\le n\le N,\left(\mu_n>0\right)\\&\psi_{n,J+\frac{1}{2}}=\psi_0+\psi_2\cdot\mathrm{T}^2\cdot e^{\mu_n}\,,\quad 1\le n\le\frac{N}{2},\left(\mu_n<0\right)\end{aligned} \tag{7}$$

Eq. (6) and Eq. (7) can be used to initialize the transport solver to obtain the numerical solution and to calculate the global normalized error, i.e. root mean square (RMS) at successive refinements. A summary of the convergence study is shown in Table 4 (LHS) and a visualization of the solution is shown below on the left hand side of Figure 7.

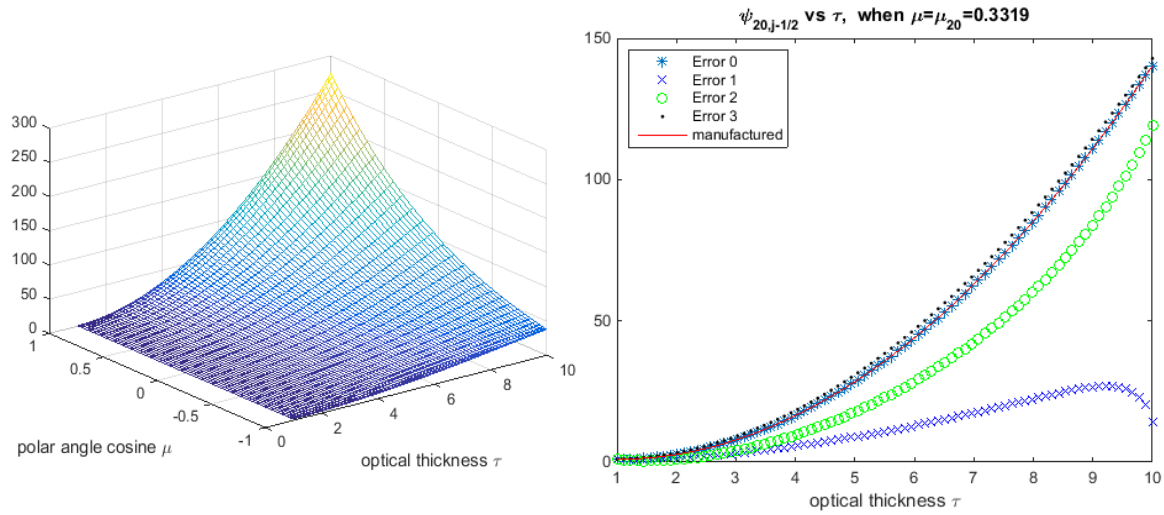

Figure 7. Angular flux (left), Numerical solutions from various implementations (right)

The value of MMS can then be demonstrated by introducing three different types of error: Error 1: sign error, Error 2: typo in a constant, Error 3: algorithmic error (Error 0: no error). The numerical solutions of all cases, together with the analytical solution are plotted on the right hand side of the Figure 7. As indicated, the numerical solution from case 3 is very small and the error from case 2 could be difficult to detect. However, because of the large sensitivity of p (order of accuracy) to all types of errors (See Table 1 RHS), it is possible to identify the existence of error in all implementations.

Table 4. Convergence Study (LHS) and Summary of Error (RHS) for the MMS Example

step size h	Nsteps	RMS	p
1	10	0.18123	1.991
0.5	20	0.04570	1.995
0.25	40	0.01149	1.997
0.125	80	0.00288	1.998
0.0625	160	0.00072	1.998
0.03125	320	0.00018	

Error	n	RMS	p
0	40	0.0115	1.997
	80	0.0029	
1	40	49.7842	1.007
	80	49.0626	
2	40	16.2230	0.992
	80	16.4865	
3	40	5.2233	1.429
	80	2.5590	

Plan of application of MMS in MPACT

Because of its relative simplicity and flexibility, the Method of Manufactured Solutions has the potential to be very effective for solution verification of a complex computer code such as MPACT. Preliminary assessments are being performed with a 1D Sn solver for both fixed source and eigenvalue problem solvers to identify the scope of problems that can be addressed in MPACT. However, some issues will need to be resolved when going from 1D to 2D, from a single group to multi-group, and from a standard finite difference spatial discretization to MOC ray tracing. Since

the MPACT configuration is more complicated than that in a simplified 1D Sn model, the approach will be to begin with simpler cases such as a 2D one group fixed source problem and then increase the complexity to multi-group and finally eigenvalue problems. However, it is apparent that MMS can be used to formally quantify the rate of the convergence of the solution to MOC parameters including geometry discretization -radial and azimuthal discretization, ray spacing, angular quadrature set, as well as the coupling between all the discretization parameters. After analyzing the 2D MOC solver, the work will be extended to the investigation of the 2D-1D solution method. A manufactured three dimensional solution will be necessary to evaluate the capability of 2D-1D scheme to resolve the axial dependence. Regarding code development, some minor modifications will be necessary to implement MMS in MPACT such as the ability to treat a generalized fixed source and with arbitrary boundary conditions. However, it is anticipated that overall benefit of an automated MMS capability to solution verification in MPACT will be well worth the effort.

3 VALIDATION

As discussed in [Oberkampf, 2004], the process of determining the degree to which a computational model provides an accurate representation of the real world from the perspective of the intended uses of the code is generally referred to as validation. This is depicted in the following schematic taken from the same reference.

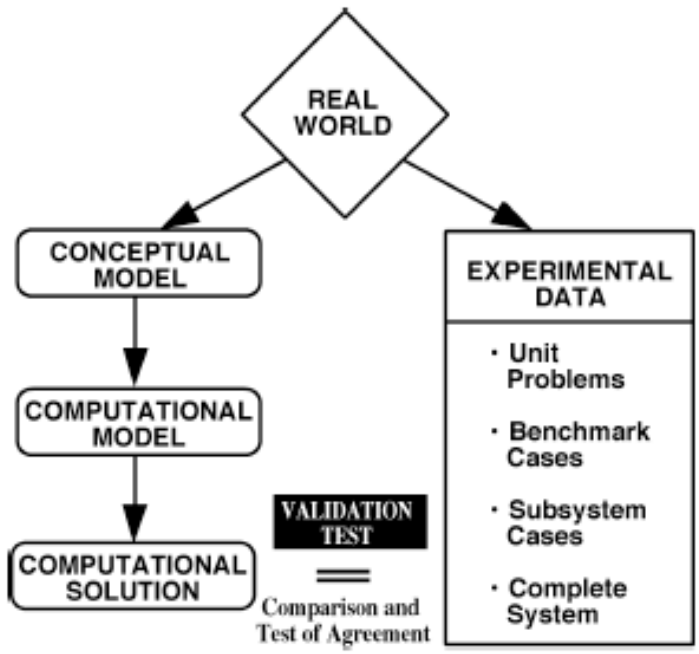

The goal of MPACT validation has been to identify those validation tests which will increase confidence in the quantitative predictive capability of the code for practical reactor applications. This section will summarize some of the preliminary work performed during Phase I of CASL on MPACT validation. The next section will summarize some of the work performed in [Godfrey, 2014] and documented in CASL-U-2014-0185-000 that has established the roadmap for MPACT validation. The subsequent sections will then review some of the preliminary work performed on each of the validation areas.

3.1 Background

A comprehensive validation plan was developed for VERA-CS [Godfrey, 2014] and presented in detail in CASL-U-2014-0185-000. This section will briefly summarize some aspects of that validation plan that are relevant to MPACT, to include the validation matrix proposed for the VERA-CS reactor neutronics codes. The four principal validation components identified in the plan are shown in Figure 8 which was reproduced from [Godfrey, 2014].

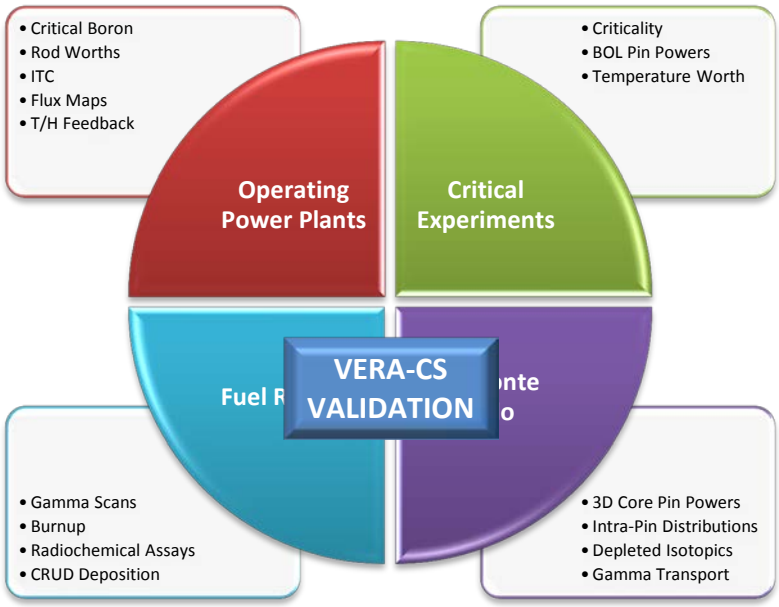

Figure 8. Four Components of VERA-CS Validation [Godfrey, 2014]

As shown in the Figure 8, MPACT results will be compared to the following sources:

1) Measured data from experiments with small critical nuclear reactors. This includes critical conditions, fuel rod fission rate distributions, control rod or burnable poison worths, and isothermal temperature coefficients.
2) Measured data from operating nuclear power plants. This includes critical soluble boron concentrations, beginning-of-cycle (BOC) physics parameters such as control rod worths and temperature coefficients, and measured fission rate responses from in-core instrumentation.
3) Measured isotopics in fuel after being irradiated in a nuclear power plant. This includes gamma scans of ^{137}Cs activity, burnup based on ^{148}Nd concentrations, and full radiochemical assays (RCA) of the major actinides and fission products.
4) Calculated quantities on fine scales from continuous energy (CE) Monte Carlo methods. This includes 3D core pin-by-pin fission rates at operating conditions, intra-pin distributions of fission and capture rates, reactivity and pin power distributions of depleted fuel, and support for other capabilities such as gamma transport and thick radial core support structure effects, for which there is currently no known measurements to benchmark against.

During the first phase of CASL, progress has been made in each of these areas, with the exception of fuel depletion / measured isotopics in item 3. The "neutronics-only" validation cases in item 1 included both those which could be simulated with the VERA-CS input as well as those which required the use of the native MPACT input. And to the extent possible, the validation cases performed in item 2 have been performed using the integrated core simulator MPACT / COBRA-TF.

The comprehensive validation matrix constructed by Godfey based on these four general areas is shown in Figure 8, which compares the required capabilities, features, and the application range of VERA-CS neutronics codes to the proposed benchmarking activities. The purpose of this Figure

was to provide a guide in prioritizing validation activities to ensure that sufficient effort is performed across the full range of capabilities and features required of a core simulator.

In Figure 9, the capabilities desired for coverage are listed on the left, and the validation activities, described in detail in Sections 3 through 0, are shown across the top. Coverage is indicated by an 'X' in the corresponding row and column positions. The optional activities (mostly critical experiments) are shaded. In general, the priorities for the activities for each component are decreasing from left to right, meaning the cases on the left side of each section should be performed first. Ideally, all capabilities should be covered by at least one activity, however due to budget and time constraints, during the first phase of CASL only selected activities listed in the matrix could be performed.

	Validation Activities																																	
	Operating Power Plants								Critical Experiments																		Post-Irradiation Exams					CE Monte Carlo			
Capabilities	Watts Bar	BEAVRS	Catawba	McGuire	Westinghouse 3-Loop	Krsko	B&W-Type	CE-Type	B&W	Helstrand	KRITZ	DIMPLE	VENUS	IPEN/MB-01	RPI	SPERT III	Strawbridge & Barry	Saxton	CREOLE	EPICURE	CAMELEON	CROCUS	JAERI TCA	ICSBEP	Catawba MOX LTAs	Three Mile Island	MAUBU	Robinson	Calvert Cliffs	Pin-by-Pin Fission Rates	Intra-Pin Distributions	Depleted Isotopics	Misc. Applications
PWR Types																																		
Westinghouse 4-Loop	X	X	X	X																					X					X			
Westinghouse 3-Loop					X								X															X					
Westinghouse 2-Loop						X																								X			
Babcock & Wilcox (B&W)							X																			X							
Combustion Engineering (CE)								X							X														X				
Fuel Assembly Types																																		
17x17	X	X	X	X	X				X										X						X					X	X	X	
16x16						X																								X			
16x16 CE								X	X						X																		
15x15					X																						X	X					
15x15 B&W							X		X																	X							
14x14 CE								X							X														X				
Mixed Oxide Fuel (MOX)			X								X		X					X	X	X					X		X						
Burnable Poison Types																																		
Pyrex	X	X	X	X	X	X			X											X										X			
IFBA	X		X	X	X	X																			X					X			
WABA	X		X	X	X																				X					X			
Solid B4C-AL2O3							X	X																	X	X			X				
Gadolinia							X		X				X							X	X		X			X	X						
Erbia								X							X																		
Control Rod Types																																		
AIC	X	X	X	X	X	X	X		X					X				X		X	X					X				X			
B4C	X		X					X	X					X						X	X	X											
Hybrid	X		X																						X					X			
Gray							X														X					X				X			
Hafnium					X																												
Incore Instrument Types																																		
Moveable	X	X	X	X	X	X																			X					X			
Fixed	X						X	X	X																	X							
Radial Reflector Types																																		
Thin Baffle	X	X	X	X	X	X	X	X				X	X												X	X				X			
Thick (Heavy) Shroud																																		X
Physics Components																																		
Neutron Transport	X	X	X	X	X	X	X	X	X	X	X	X	X	X	X	X	X	X	X	X	X	X	X	X	X	X	X	X	X	X	X	X	X
Gamma Transport																																	X
Coolant Density Feedback	X	X	X	X	X	X	X	X			X								X				X		X	X	X	X	X	X			
Fuel Temperature Feedback	X	X	X	X	X	X	X	X			X								X				X		X	X	X	X	X	X	X		
Isotopic Depletion	X	X	X	X	X	X	X	X																	X	X	X	X	X		X	X	
Xenon Concentration	X	X	X	X	X	X	X	X																								X	
Shutdown Decay	X	X	X	X	X	X	X	X																	X	X	X	X	X				
Physics Results																																		
Reactivity	X	X	X	X	X	X	X	X	X		X	X	X	X	X	X	X	X	X	X	X	X	X	X	X					X	X	X	
Assembly Power Distribution	X	X	X	X	X	X	X	X																	X					X			
Pin Power Distribution									X		X	X	X	X	X			X	X	X	X									X	X	X	
Intra-Pin Power Distribution																															X		
Pin Burnup Distribution																									X	X	X	X	X		X		
Intra-Pin Burnup Distribution																													X		X		
Incore Instrumentation Response	X	X	X	X	X	X	X	X	X				X						X						X	X							
Excore Instrumentation Response			X	X								X	X																				X
Control Rod Worth	X	X	X	X	X	X	X	X	X									X		X	X	X			X					X			
Temperature Coefficient	X	X	X	X	X	X	X	X			X			X					X				X		X								

Figure 9. VERA-CS Validation Assessment Matrix [Godfrey, 2014]

3.2 Validation Activities in MPACT During CASL Phase I

During the past year, selected activities from this validation matrix have been included as part of the normal code development tasks in both PHI and RTM. A sample of the ticket tracking from PHI is shown in Table 5 which was extracted from the PHI VERA-CS developer website.

Table 5. Sample PHI KANBAN Ticket Tracking Validation Activities in MPACT

Ticket	Summary	Priorty	Status	Type	Owner	Supports Milestones	Modified
#3551	Run BEAVRS Benchmark Cycle 2	P1	in_prog	story	bn7	L2.PHI. P10.01	Mar 11, 2015
#3478	Depletion Verification by comparison to Triton	P2	in_prog	story	ww5	L3.PHI.VCS. P11.02	Feb 5, 2015
#3580	Validate MPACT with B&W criticals	P2	in_prog	story	zjx		Apr 14, 2015
#3665	Validate with EPRI Depletion Benchmark	P4	in_prog	story	ykk		Apr 11, 2015

Additional MPACT validation activities have been performed in RTM, to include several of the VERA Benchmark activities based on Watts Bar Unit I data, as well as the benchmarking of MPACT using the SPERT critical data. Reports and publications have been prepared as part of both these PHI and RTM validation activities and the following sections will summarize some the work included in those reports. However, the readers are referred to the CASL reports for more detailed information.

3.2.1 Critical Experiments

Critical experiments are small nuclear reactors typically designed to provide validation data for nuclear methods and software, particularly for materials and geometries similar to those found in operating nuclear power plants. These experiments are usually performed without power at isothermal conditions and without fuel depletion. During Phase I of CASL, work was performed on the B&W critical experiments which are among the most widely analyzed critical experiments in the LWR industry. Additionally, as part of work being performed in the development of transient methods in MPACT, work was performed on the critical condition of the Special Power Excursion

Reactor Test (SPERT) reactor. The following section will summarize the work performed on both of these tests.

3.2.1.1 Babcock & Wilcox Critical Experiments

The B&W critical experiments most relevant to MPACT validation are the 1484 Fuel Storage experiments and the 1810 series of BOL reactor experiments. Initial results have been prepared on both experiments with MPACT and reported in CASL-U-2015-XXXX-000 [Kulesza, 2015].

1484 – Fuel Storage Experiments

The Babcock & Wilcox 1484 critical experiments were designed to provide criticality data to support the long term storage of LWR fuel in spent fuel pools. A total of 20 critical configurations were constructed to provide measured benchmark data for validation of nuclear codes. The report for the experiments, funded by what is now the U.S. Department of Energy (DOE), was released in 1979 [Baldwin, 1979].

The twenty critical configurations were built in a core tank with low enriched (2.46%) UO2 fuel rods and water as the neutron moderator. The rods were clustered into nine LWR-like assemblies in a 3x3 configuration, with variable spacing in between the assemblies, as shown in Figure 10. In some configurations, stainless steel or borated aluminum sheets are placed in between the assemblies to simulate a spent for storage configuration. Therefore only a subset of the experiments is consistent with power plant geometries for validation.

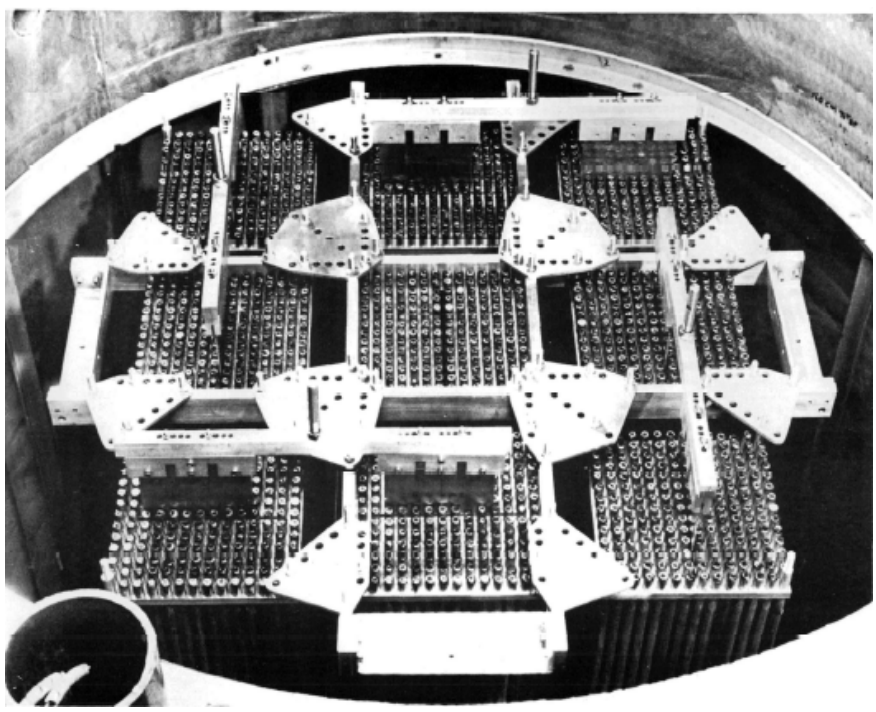

Figure 10. B&W Critical Experiment Facility

The B&W-1484 experiment consisted of 21 critical configurations (listed here as 4:1 – 4:21) that simulated a variety of close-packed light water reactor (LWR) fuel storage configurations. Criticality measurements were performed and a series of Monte Carlo criticality calculations were also performed at the time to create an analytical basis for comparison with the experimental data. Core 4:1 is a reference "core" containing 438 fuel rods arranged in a roughly cylindrical configuration. All of the remaining cores consist of nine 17 × 17 fuel pin assemblies grouped into a 3 × 3 array and spaced from 0 to 4 pin pitches apart. From this set of experiments, Cores 4:1 and 4.2 were determined to be the most appropriate for the initial phase of MPACT validation and results will be summarized here. Most of the other cases represent configurations that are not appropriate to assess a core simulator with but rather are appropriate for assessing spent fuel pool calculation codes. However, Core 4:3 is also currently being analyzed and will be included in a future update to this document.

All calculations were performed with MPACT using the 2-D method of characteristics (MOC) with an axial buckling to represent the axial leakage. In addition to MPACT, the 3D generalized geometry Monte Carlo computer code KENO was used to rerun the cases prepared as part of the original benchmarking effort for Cores 4:1 and 4:2. The details of both the MPACT and KENO models is provided in CASL-U-2015-XXXX-000 [Kulesza, 2015].

B&W Core 1484 Geometry/Materials

The geometry and material distribution plan views of Cores 4:1 and 4:2 are shown in the top and bottom, respectively, of Figure 11. In these figures, the fuel is red, the cladding is green, and the moderator as blue. Taking advantage of geometric symmetry, Core 4:1 is a half-core reflective model and core 4:2 is a quarter-core reflective model.

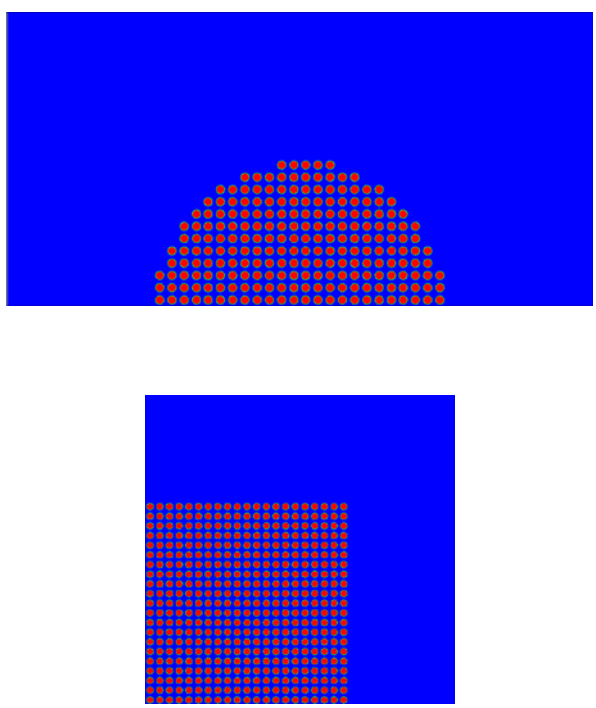

Figure 11. B&W-1484 Core 4:1 (Top) Core 4:2 (Bottom)

The cases were performed using the standard MPACT 47-group library, and as discussed in the report some adjustments were made for selected materials which were not available in the library. Axial buckling was used to represent the axial leakage effects and buckling values for Core 4:1 and 4:2 were recomputed based on a nominal 2.025 cm extrapolation length for Core 4:1 with the same buckling value assumed for Core 4:2 because of the similarity in the moderator height. The buckling values used are summarized in Table 6.

Table 6. Summary of Geometric Buckling & Critical Height Values

Core	Geometric Buckling (cm^{-2})	Critical Height (cm)	Buckled Height (cm)	Extrapolation (cm)
4:1	4.51e-4	143.88	147.93	4.05
4:2	4.51e-4	144.29	147.93	3.64

The eigenvalues for Cores 4:1 and 4:2 are shown in Table 7 which shows the effect of different scattering methods used in MPACT. The scattering methods included:

1. P_2 which is the standard scattering expansions for neutron transport calculations,
2. TCP_0 (NLC), which calculates a diffusion coefficient based on a total neutron leakage conservation through a uniform slab of hydrogen [Herman, 2013]
3. TCP_0 (Out-scatter), which performs a traditional out-scatter correction whereby the transport-corrected cross section is the total cross section for a given group with all first-moment scattering to other groups subtracted out.

Table 7. B&W-1484 Core 4:1 and 4:2 MPACT-Calculated Eigenvalues

Calculated Effective Eigenvalue		
Scattering Method	**Core 4:1**	**Core 4:2**
P_2	0.99993	0.99761
TCP_0 (NLC)	0.99838	0.99597
TCP_0 (Out-scatter)	0.99152	0.99343
Distance from Critical (pcm)		
Scattering Method	**Core 4:1**	**Core 4:2**
P_2	-7	-239
TCP_0 (NLC)	-162	-403
TCP_0 (Out-scatter)	-848	-657

As expected P_2 is the most accurate for Core 4:1 (~10 pcm) and slightly less accurate for Core 4:2 (~250 pcm). However, the computationally more efficient TCP_0 NLC-based transport-corrected scattering methods still provides good results, especially for Core 4:1. Some of the bias in Core 4:2 compare to Core 4:1 is likely attributable to differences in the composition and the buckling treatment. Core 4:1 has unborated moderator whereas Core 4:2 has 1037 ppm of dissolved boron. In prior analyses, discrepancies have been observed based on the use of a historic B-10:B-11 ratio versus a more modern ratio (i.e., 19.9:80.1, respectively). However, the MPACT calculation used the same ratio as the historic KENO executions.

The radial and azimuthal mesh definitions for Cores 4:1 and 4:2 are consistent and a sensitivity study was performed which showed no significant changes (i.e., improvements) when varying the MOC discretization. A similar sensitivity study was performed in the ray spacing without significant improvement in the calculated effective eigenvalues. However, it should be noted the buckling value for Core 4:1 was recomputed and Core 4:2 is assumed to be the same because no historic value is available for comparison. Because the buckling, and thus leakage, will directly influence the eigenvalue, additional work will be performed to develop a rigorous method to (re-)compute the buckling values on a core-wise basis for this benchmark problem.

In summary, the benchmark models for Cores 4:1 and 4:2 generally produce effective eigenvalues within 200 pcm of measured values for all scattering treatments. Core 4:2 exhibits a lower calculated eigenvalue (~200 pcm) versus measurement. The major unknown is with respect to the applied buckling value which has a direct impact on the effective eigenvalue. As such, additional effort to rigorously calculate this buckling value will performed on a case-by-case basis using a more physically-appropriate method than a slab approximation.

B&W-1810 Critical Experiments

The B&W 1810 series of critical experiments were developed by B&W, Duke Power, and DOE to provide beginning-of-life (BOL) benchmark data to support the development of an advanced PWR fuel assembly for extended fuel burnup [Newman, 1984]. Twenty-three core configurations were constructed, and the following measurements were taken:

a. Reactivity worths of gadolinia, control, and void rods
b. Core radial power distribution
c. Radial power profiles within a UO2 pellet containing gadolinia
d. 238U resonance integrals for solid and annual fuel pellets
e. Rhodium in-core detector signals

The experiments were performed at B&W's Lynchburg Research Center using UO2 fuel rods with 2.46% and 4.02% U235 enrichment. Both solid and annular rods containing 4.0% gadolinia were included in some of the arrangements, and Ag-In-Cd (AIC) and B4C control rods were also used. The rods were arranged inside of a large core tank with variable moderator height. In some cases, multiple fuel rods were removed to simulate the large water rods similar to the Combustion Engineering (CE) lattice design. A sample core configuration is shown in Figure 12.

Table 8 shows a summary of 19 different core configurations assessed in CASL-U-2015-XXXX-XX [Kulesza, 2015], all of which have varying layouts of fuel and burnable absorber rods. Additionally, select cases also have control rods inserted, of which there are two types (Ag-In-Cd also commonly referred to as AIC and B_4C). There were a variety of materials used in these cases, including three different fuel compositions, two burnable absorber materials, and a handful of different metals for fuel rod cladding and detector modeling. The detailed VERA input for each of these cases is provided in the CASL report. Lastly, the boron concentration of the coolant was adjusted in the experiment until a critical configuration was obtained. All of these cases were simulated in 2D with a prescribed axial buckling value of 4.1×10^{-4} cm^2 to account for the 3D effect. All cases were run using the same 47-group ORNL library as used in the 1484 cases.

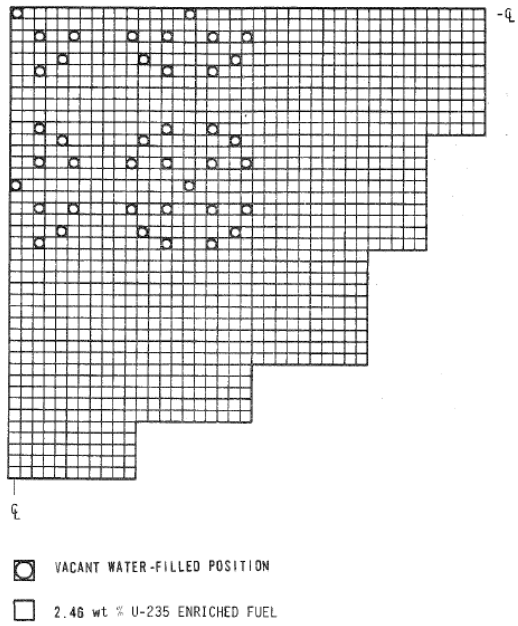

Figure 12. B&W-1810 Core 8:1 Layout

Table 8. B&W-1810 Benchmark Configuration Summary

Core	Short Description	2.46% Pins	4.02% Pins	Gd Pins	B_4C Pins	AIC Pins	Water Holes	Boron (ppm)
1	**0 Gd**	4808	0	0	0	0	153	1337.9
2	**0 Gd, AIC Rods**	4808	0	0	0	16	137	1250.0
3	**20 Gd**	4788	0	20	0	0	153	1329.3
4	**20 Gd, AIC Rods**	4788	0	20	0	16	137	1171.7
5	**28 Gd**	4780	0	28	0	0	153	1208.0
5A	**32 Gd**	4776	0	28	0	0	153	1191.3
5B	**28 Gd**	4780	0	32	0	0	153	1207.1
6	**28 Gd, AIC Rods**	4780	0	28	0	16	137	1155.8
6A	**32 Gd, AIC Rods**	4776	0	32	0	16	137	1135.6
7	**28 Gd (annular)**	4780	0	28 (ann.)	0	0	153	1208.8
8	**36 Gd**	4772	0	36	0	0	153	1170.7
9	**36 Gd, AIC Rods**	4772	0	36	0	16	137	1130.5
10	**36 Gd, Void Rods**	4772	0	36	0	0	137	1177.1
12	**0 Gd**	3920	0	0	0	0	153	1899.3
13	**0 Gd, B4C Rods**	3920	888	0	16	0	137	1635.4
14	**28 Gd**	3920	888	28	0	0	153	1653.8
15	**28 Gd, B4C Rods**	3920	860	28	16	0	137	1479.7
16	**36 Gd**	3920	852	36	0	0	153	1579.4
17	**36 Gd, B4C Rods**	3920	852	36	16	0	137	1432.1

Results

The results for the various core configurations are shown in Table 9. As all configurations should be critical, the difference reported is just the eigenvalue difference from unity. In general, there is a clear bias in the TCP_0 results, which tend to be 150-200 pcm low. A similar trend is observed with P_2 scattering, where Cores 8:1 – 8:10 have roughly a -100 pcm bias, though the eigenvalue for Cores 8:12 – 8:17 tend to be a bit higher than critical. The standard deviation, root mean square, and maximum errors are summarized as well.

Table 9. B&W-1810 Benchmark Results

Core	Short Description	TCP0		P2	
		Eig.	Diff. (pcm)	Eig.	Diff. (pcm)
1	0 Gd	0.99809	-191	0.99981	-19
2	0 Gd, AIC Rods	0.99757	-243	0.99915	-85
3	20 Gd	0.99778	-222	0.99933	-67
4	20 Gd, AIC Rods	0.99840	-160	0.99990	-10
5	28 Gd	0.99749	-251	0.99899	-101
5A	32 Gd	0.99739	-261	0.99888	-112
5B	28 Gd	0.99755	-245	0.99905	-95
6	28 Gd, AIC Rods	0.99770	-230	0.99918	-82
6A	32 Gd, AIC Rods	0.99765	-235	0.99912	-88
7	28 Gd (annular)	0.99749	-251	0.99899	-101
8	36 Gd	0.99762	-238	0.99910	-90
9	36 Gd, AIC Rods	0.99752	-248	0.99900	-100
10	36 Gd, Void Rods	0.99743	-257	0.99889	-111
12	0 Gd	0.99886	-114	1.00092	92
13	0 Gd, B4C Rods	0.99901	-99	1.00056	56
14	28 Gd	0.99854	-146	1.00024	24
15	28 Gd, B4C Rods	0.99887	-113	1.00030	30
16	36 Gd	0.99851	-149	1.00015	15
17	36 Gd, B4C Rods	0.99848	-152	0.99990	-10
Cores 1-10	2.46% Enriched Throughout	STDDEV	29	STDDEV	32
		RMS	235	RMS	87
		MAX	261	MAX	112
Cores 12-17	4.02% Enriched Inner Core, 2.46% Outer	STDDEV	23	STDDEV	35
		RMS	131	RMS	47
		MAX	152	MAX	92
Total		STDDEV	56	STDDEV	64
		RMS	208	RMS	77
		MAX	261	MAX	112

Figure 13, Figure 14 and Figure 15 show the difference in the midplane fission rate distributions. In the figures for Cores 8:5 and 8:14, the burnable absorber pins are highlighted with a purple boundary. In general, the results look good, but additional work will be performed on each of the benchmarks.

TCP0

0.08	0.26						
-0.53	-0.45						
0.40	0.57	0.22	0.88				
0.59	0.56	-0.46	-0.16				
-0.84	-0.99		-0.29	-0.34	-0.28		
-0.11	-1.27	0.45	0.31	0.05	0.51	0.10	
-0.14	0.33	0.27	0.17	0.14	0.11	-0.02	0.16

RMS 0.47%
MAX 1.27%

P2

0.08	0.28						
-0.48	-0.42						
0.43	0.63	0.36	1.08				
0.61	0.62	-0.31	0.01				
-0.82	-0.99		-0.20	-0.25	-0.27		
-0.16	-1.32	0.42	0.33	0.05	0.44	-0.03	
-0.26	0.23	0.21	0.11	0.05	-0.02	-0.18	-0.02

RMS 0.48%
MAX 1.32%

Figure 13. B&W-1810 Core 8:1 Fission Rate Difference, Center Assembly

TCP0

-0.15	0.70						
0.24	0.15						
0.82	-0.63	-0.29	0.12				
0.18	0.27	-0.46	-0.33				
1.29	-0.51		0.34	-1.19	0.33		
1.03	0.41	-0.47	0.53	-0.14	-0.17	-0.06	
1.21	0.07	-0.21	-0.09	-0.30	-0.20	-0.04	-0.02

RMS 0.54%
MAX 1.29%

P2

-0.23	0.66						
0.14	0.10						
0.80	-0.74	-0.34	0.14				
0.08	0.29	-0.35	-0.26				
1.31	-0.47		0.43	-1.17	0.35		
1.01	0.42	-0.43	0.63	-0.09	-0.27	-0.12	
1.15	0.05	-0.17	-0.04	-0.28	-0.25	-0.08	-0.03

RMS 0.53%
MAX 1.31%

Figure 14. B&W-1810 Core 8:5 Fission Rate Difference, Center Assembly

TCP0

0.07	0.16						
-0.40	-0.88						
0.58	0.08	1.20	0.49				
-1.99	-0.13	0.08	-0.09				
-0.76	-0.15		0.50	-0.48	1.10		
-0.38	-0.38	1.32	0.20	0.22	0.98	-0.16	
-0.31	-0.33	-1.36	0.61	0.14	-0.55	0.20	-0.81

RMS 0.70%
MAX 1.99%

P2

0.08	0.18						
-0.32	-0.82						
0.58	0.13	1.40	0.72				
-2.00	-0.08	0.30	0.15				
-0.75	-0.13		0.66	-0.35	1.10		
-0.47	-0.45	1.32	0.21	0.21	0.87	-0.33	
-0.48	-0.47	-1.44	0.51	0.00	-0.72	-0.01	-1.03

RMS 0.74%
MAX 2.00%

Figure 15. B&W-1810 Core 8:12 Fission Rate Difference, Center Assembly

3.2.2.2 The Special Power Excursion Reactor Test (SPERT)

The SPERT Project was established as part of the U. S. Atomic Energy Commission's reactor safety program in 1954, with the objective of providing experimental and theoretical investigations of the kinetic behavior and safety of nuclear reactors. The SPERT III pressurized water reactor [Durgone, 1965] was constructed as a part of this safety program to fulfill the need for a facility in which to conduct reactor kinetic behavior and safety investigations under operating conditions. The facility was designed and incorporated essential features typical of pressurized-water and boiling-water reactors. Among several core designs, the E-Core consisting of 60 assemblies was employed to perform several reactivity insertion accident (RIA) experiments. The data measured during the experiments was available to validate neutronics codes for both steady-state and transient core conditions. However, prior to performing any of the RIA experiments, a series of critical experiments at Cold Zero Power (CZP) and Hot Zero Power (HZP) were performed and were the focus of the validation work using SPERT during Phase I of CASL.

Models of SPERT were developed with both MPACT and KENO V.a, which is a three-dimensional Continuous Energy Monte Carlo criticality transport program developed and maintained as part of the SCALE code package [Bowman, 2011]. The principal motivation of using KENO was to establish a steady-state Monte Carlo model for the SPERT III E-Core which could provide very detailed fission rates throughout the reactor to complement the experimental measurements.

Core specifications

The SPERT III E-core is a small, low-enriched UO_2 fueled PWR core with the general neutronics characteristics of a commercial power reactor without a significant fission product inventory. The cross section of the core is illustrated in Figure 16 and consists of 60 fuel assemblies, which are surrounded by different shapes of filler pieces and four rings of thermal shield, and housed by the reactor vessel. There are 48 fuel assemblies, each containing 25 fuel rods in a 5 by 5 rectangular array with a square pitch of 1.4859 cm. There are 12 smaller fuel assembly cans 6.35 cm on a side, each containing 16 fuel rods arranged in a 4 by 4 rectangular array with the same pitch as the 25-rod assemblies. Four of the 16-rod assemblies surround the centrally located transient rod guide, and the remaining eight 16-rod assemblies form fuel followers of the eight E-core control rods. Four pairs of control rods and a cruciform-shaped transient rod are loaded in the core. The main design characteristics of the E-core are presented in Table 10. Other detailed core parameters can be found in the reference [Durgone, 1965].

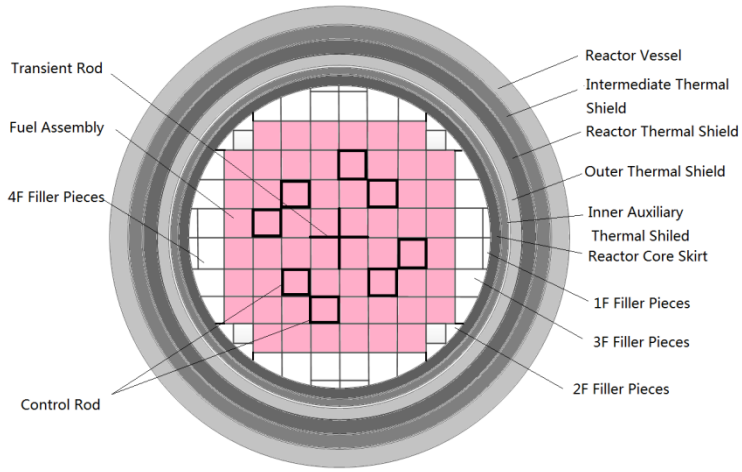

Figure 16. SPERT III E-core cross-section.

Table 10. Basic Core / Fuel Data for SPERT III E-core

Parameters	Value
Reactor type	Experimental PWR
Moderator/Coolant	H_2O/H_2O
Core rated power	20 MW
Core equivalent diameter	0.66 m
Active height	97.282 cm
Fuel rod outer diameter	1.1836 cm
Fuel rod inner diameter	1.0820 cm
Fuel pellet diameter	1.0668 cm
Fuel rod pitch	1.4859 cm
Fuel enrichment	4.8 wt% enriched UO_2 (10.5 g/cm^3)
Fuel tube	Stainless steel, type 348
Gas gap	Helium
Control rods composition	Absorber section 1.35 wt% ^{10}B in Type 18-8 stainless steel; 0.4724 cm thick hollow square box
25-rod fuel assembly	7.5565*7.5565*130.175 cm
16-rod fuel assembly	6.3398*6.3398*130.175 cm
CR with fuel followers	6.2890*6.2890*112.673 cm
Fuel assembly pitch	7.62 cm
Filler pieces thickness	0.3175 cm
Assembly box thickness	0.3175 cm

The 25-rod assembly is modeled as shown in Figure 17. The inner part of the 25-rod assembly model consists of 10×10 quarter fuel pins. This array is surrounded by a 0.0635 cm thick can and 0.03175 cm of bypass water outside the can. The can and bypass water together form one layer of MPACT pins. Therefore, the 25-rod assembly is divided into a 12×12 array of pin mesh with the thicknesses of the inner pin mesh of 0.74295 cm, and thicknesses of the outer pin mesh of 0.09525 cm. This meshing was also used for all other assembly models.

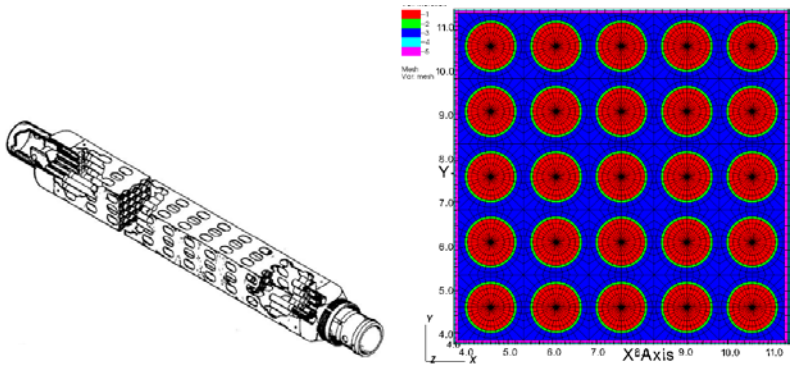

Figure 17. MPACT 25-rod Fuel Assembly Model

The core filler pieces are explicitly modeled in MPACT as shown in Figure 18. The thickness of the filler box is 0.3175 cm and the outer dimension is the same as the 25-rod fuel assembly. The curved portion of type 1F, 2F and 3F are approximated on the rectangular grid.

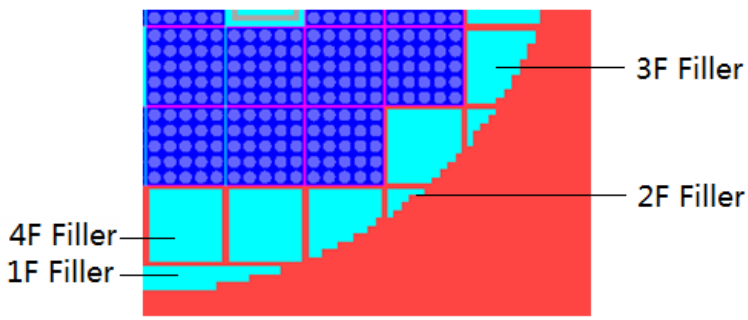

Figure 18. MPACT model for core filler

The weight of the intermediate grids is not provided in the documentation and was estimated to be 300 grams. Because the structure of the grid is too complex to model explicitly, it is homogenized with the coolant in a height of approximately 6 cm (one axial mesh). The corresponding composition of the grid is 19% steel and 81% water. The positions of the two axial grids are in the 6th and the 12th node from the bottom of the active core as shown in Figure 19.

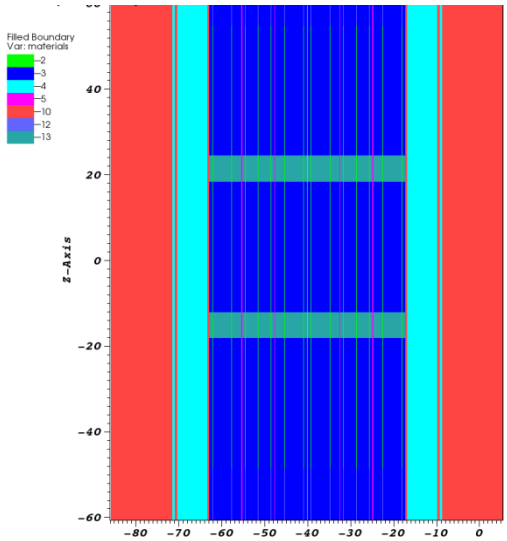

Figure 19. MPACT model for axial grids

The flux suppressors between the control rod absorbers and fuel followers were modeled explicitly. According to the documentation, the distance between the absorber and fuel follower is 11.938 cm, so the lower half of that height is filled with spring like the other fuel rods, while the upper half is filled with moderator and type 18-8 stainless steel containing 1.35 wt% B-10. While the precise geometry of the flux suppressor was not available, the volume of steel containing B-10 was preserved with the data given in the documentation. The flux suppressors were modeled as shown in Figure 20. The MPACT model for the middle of the active core is shown in Figure 21.

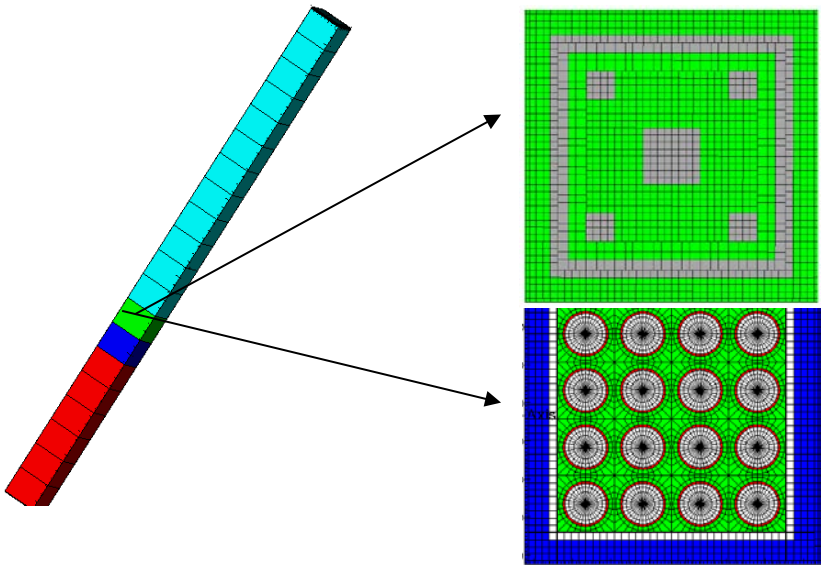

Figure 20. MPACT model for flux suppressors

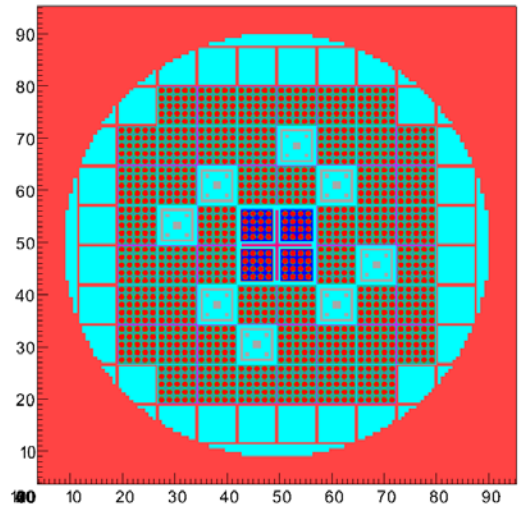

Figure 21. MPACT model for middle of active core

KENO Model of SPERT III E-core

The KENO model was developed to mimic exactly the geometry of the MPACT model. There are only three differences between the KENO and MPACT models: 1) the reactor containment vessel is explicitly modeled as a cylinder in KENO, rather than approximated on a rectangular grid as in the MPACT model; 2) the filler pieces do not closely contact the reactor skirt to avoid overlapping geometry and 3) a small gap (10^{-5} cm) is introduced between assemblies in the KENO model to ensure that boundaries of "holes" (assemblies) do not overlap. These minor discrepancies had a negligible effect on the results of the simulations. The KENO simulations were run in continuous energy mode with 5,500 generations consisting of 5×10^{6} neutrons per generation, of which 500 generations were skipped. In order to calculate pin powers throughout the core, a separate unit for each region of interest was created. KENO does provide mesh tally capabilities, but only the flux can be tallied and not reaction rates. KENO does not have the ability to explicitly calculate pin powers, and therefore fission rates were calculated instead.

MPACT and KENO Results and Analysis

The eigenvalue and critical control rod positions for the cold zero power (CZP) and hot zero power (HZP) configurations of the SPERT III E-core were calculated with MPACT and KENO. The cases were performed in MPACT using P2 scattering with 0.05 cm ray spacing, and the Chebyshev-Gauss quadrature set and 16 azimuthal and 4 polar angles per octant. The multi-group NEM kernel was used to perform the axial solution, and both CZP and HZP cases were run with 20 axial planes. Solutions were performed with the ORNL 47-group library based on ENDF-VII. The typical computational time for each case running with 720 cores is around 2 hours. The KENO cases were run with the continuous energy ENDF-VII library. The computational time of KENO with 240 cores for each case is around 150 hours. The eigenvalues for MPACT and KENO are compared in Table 11. The critical control rod positions are also compared with experiment in Table 12. Comparison of critical control rod position**,** however, only the CZP critical control rod position was calculated with KENO.

Table 11. Comparison of eigenvalues

Case	Temp. (F)	C.R. Position (cm)	MPACT	KENO-CE
CZP	70	37.0	0.99613	0.99857±0.00001
HZP	550	71.8	1.00023	1.00069±0.00001

Table 12. Comparison of critical control rod position

Case	Temperature (F)	Experiment	MPACT	KENO
CZP	70	37.0	38.2	36.3
HZP	550	71.8	74.4	-

As indicated, there is very good agreement for both eigenvalue and control rod positions with the maximum difference in eigenvalue of less than 25 pcm for HZP and less than 400 pcm for CZP. The experimental data also include the control rod worth for CZP. The calculated results of MPACT and KENO are compared against the experimental results in Figure 22 and good agreement is observed between the experimental and the MPACT and KENO results.

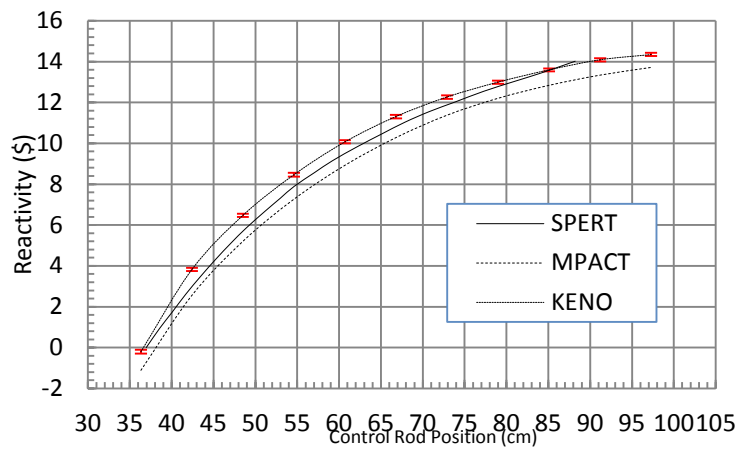

Figure 22. Comparison of control rod worth for CZP

The experimental results do not provide detailed power distribution measurements which emphasized the value of the fission rate distribution comparisons between MPACT and KENO. A comparison of the relative fission rate distributions between the two codes at CZP and HZP, are shown in Figure 23 and Figure 24, respectively. These figures include (a) the assembly-averaged fission rate distribution at the plane with the peak power (a quarter core) and (b) the pin-wise relative difference distribution between two codes at the plane with the peak power (full core).

In the CZP peak-power plane shown in Figure 23, MPACT systematically underestimates the assembly plane-averaged power by 2.5 to 5.5% relative to KENO, however the overall shape of the power distribution shows very good agreement between the two codes. As shown in Figure 23, the maximum relative difference of 6.5% occurs in the corner pin location of one of the 4 central assemblies, the same location as the peak pin power.

KENO	1.376±0.027	1.688±0.030	1.900±0.032
MPACT	1.339	1.634	1.835
Rel. Diff.	0.027	0.032	0.034
1.364±0.027	1.967±0.032	2.705±0.038	3.013±0.040
1.327	1.893	2.584	2.874
0.027	0.038	0.045	0.046
1.678±0.030	2.849±0.039	3.981±0.058	4.135±0.047
1.624	2.718	3.785	3.927
0.032	0.046	0.049	0.05
2.007±0.033	3.447±0.054	4.302±0.049	5.241±0.067
1.933	3.283	4.083	4.968
0.037	0.048	0.051	0.052

(a) Assembly-averaged fission rate distribution
Plane 5 (peak-power plane)

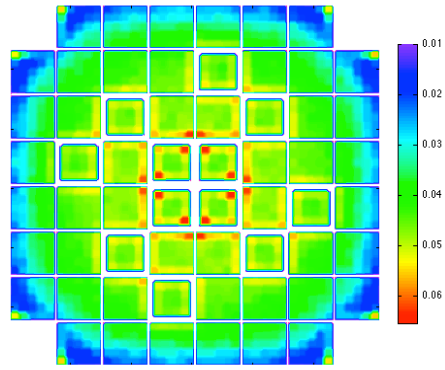

(b) Pin-wise relative difference of fission rate (Plane 5, peak-power plane)

Figure 23. Comparison of fission rate distribution– CZP

In the HZP peak-power plane shown in Figure 24, MPACT systematically underestimates the assembly plane-averaged power by up to 2.5% relative to KENO, which is a difference of less than 2σ based on the KENO uncertainty. In fact, only the difference in the four central assemblies exceeds 1σ. The overall shape of the power distribution shows very good agreement between the two codes with the maximum relative difference of about 4.7% occurring in the outermost corners of the core, where pin powers are less than a third of peak power.

KENO	0.867±0.021	0.978±0.022	1.108±0.024
MPACT	0.862	0.975	1.103
Rel. Diff.	0.6%	0.3%	0.5%
.868±0.021	1.043±0.023	1.410±0.027	1.572±0.028
0.863	1.040	1.398	1.556
0.5%	0.4%	0.8%	1.0%
1.000±0.022	1.537±0.028	2.354±0.045	2.198±0.034
.997	1.521	2.317	2.165
0.3%	1.0%	1.6%	1.5%
1.197±0.025	2.050±0.042	2.315±0.035	3.185±0.052
1.190	2.020	2.278	3.114
0.6%	1.5%	1.6%	2.2%

a.) Assembly-averaged fission rate distribution
Plane 8 (peak-power plane)

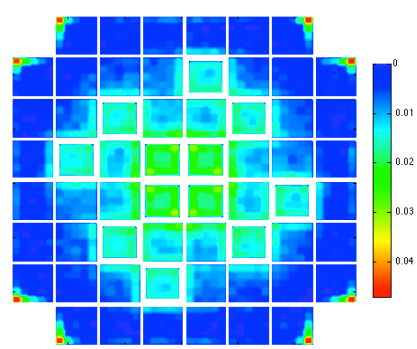

(b) Pin-wise relative difference of fission rate distribution (Plane 8, peak-power plane)

Figure 24. Comparison of fission rate distribution– HZP

Both codes predict that the pin-wise peak powers are located in the center assemblies and the pin-wise fission rate distributions are compared for the assembly with the peak power in Figure 25. It can be seen that the maximum difference is less than 6.5% for CZP and 4% for HZP. The axial relative distributions of fission rate of this peak-power assembly are compared in Figure 26 where good agreement can be observed for both CZP and HZP cases. Most of the MPACT and KENO pin powers are within 1σ of the KENO uncertainties. In fact, the relative difference between the KENO and MPACT pin powers for HZP are all well within 1σ, while a few relative differences between the KENO and MPACT pin powers for CZP exceed 1σ, but are within 1.5σ.

5.898±0.283	5.281±0.275	5.306±0.271	6.008±0.288	KENO	3.321±0.213	3.117±0.206	3.151±0.208	3.466±0.222
5.578	5.012	5.029	5.616	MPACT	3.244	3.0502	3.0801	3.3559
-5.4%	-5.1%	-5.2%	-6.5%	Rel. Diff.	-2.3%	-2.1%	-2.3%	-3.2%
5.281±0.275	4.557±0.246	4.567±0.251	5.235±0.267		3.111±0.208	2.874±0.198	2.912±0.192	3.242±0.214
5.01	4.353	4.358	4.965		3.0514	2.8257	2.8593	3.1657
-5.1%	-4.5%	-4.6%	-5.2%		-1.9%	-1.7%	-1.8%	-2.4%
5.306±0.276	4.568±0.251	4.549±0.250	5.185±0.264		3.151±0.211	2.911±0.204	2.944±0.203	3.266±0.209
5.027	4.357	4.347	4.93		3.0815	2.8596	2.8931	3.1952
-5.3%	-4.6%	-4.4%	-4.9%		-2.2%	-1.8%	-1.7%	-2.2%
5.998±0.288	5.235±0.267	5.185±0.264	5.692±0.279		3.460±0.218	3.242±0.207	3.262±0.215	3.527±0.219
5.615	4.964	4.929	5.403		3.3567	3.1659	3.1953	3.447
-6.4%	-5.2%	-4.9%	-5.1%		-3.0%	-2.3%	-2.0%	-2.3%

(a) CZP (b) HZP

Figure 25. Comparison of pin-wise fission rates of the peak power assemblies

The axial fission rate distributions predicted by MPACT and KENO for CZP and HZP are compared in Figure 26. As indicated, there is generally very good agreement with a slight underprediction by MPACT of the peak power for the CZP condition.

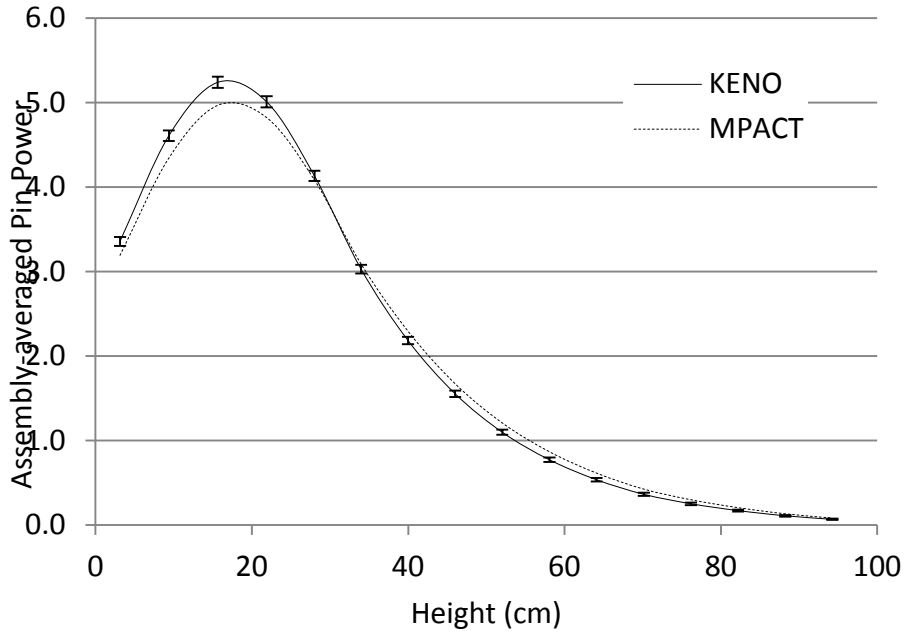

(a) CZP

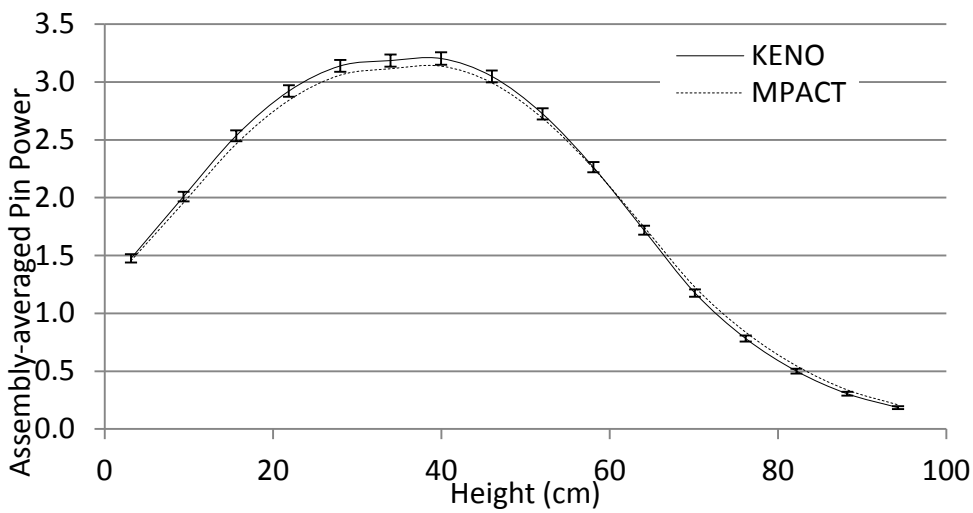

(b) HZP

Figure 26. Axial fission rates distribution

Overall, KENO and MPACT have the same magnitude of discrepancies in both eigenvalues and control rod worth compared with the experimental data. Because better agreements are observed for HZP condition than for the CZP condition, it appears some improvements in the nuclear data library might be needed for Cold conditions.

The MPACT and KENO results for the SPERT experiments support the following conclusions:

1) The detailed three-dimensional heterogeneous modeling of complex reactor is feasible for both the deterministic code MPACT and the Monte-Carlo Code KENO.
2) Detailed geometry descriptions of in-core components are very important for steady-state validation.
3) The SPERT III E-Core experiment can be used as a benchmark for high-fidelity simulation of light water reactors.

4) Both KENO and MPACT can provide good results for the k_{eff} of both CZP and HZP cases. The fission rates distribution agrees well between KENO and MPACT except in some regions with very low relative power.

3.2.2 Operating Power Plants

Measurement data from operating nuclear power plants provides the broadest range of core simulator validation data. The CASL consortium is working with several stakeholders who own and/or operate PWR power plants and some of that data has become available for validation of MPACT.

3.2.2.1 Watts Bar Nuclear Plant

The Watts Bar Nuclear Plant in Spring City, TN is owned and operated by the Tennessee Valley Authority (TVA), a CASL core partner. Watts Bar was selected as CASL's "Physical Reactor" for initial benchmarking activities. Unit 1 was the last commercial nuclear unit to come online in the 20th century, and Unit 2 will be the first to come online in the 21st century.

Watts Bar Nuclear Unit 1 (WBN1) is a traditional Westinghouse 4-loop PWR with an ice condenser containment design, one of the most common reactor designs in the U.S. today. It is currently licensed to 3459 MWth power and is currently operating Cycle 13. WBN1 has 193 fuel assemblies of the 17x17 type, has used Pyrex, IFBA, and WABA burnable poisons, and has 57 AIC/B4C hybrid rod cluster control assemblies (RCCAs). It has a moveable in-core detector system for power distribution measurement. WBN1 is also the only commercial reactor in the U.S. to contain Tritium Producing Burnable Absorber Rods (TPBARs) for the DOE/NNSA's tritium program. A schematic of the core loading is shown in Figure 27.

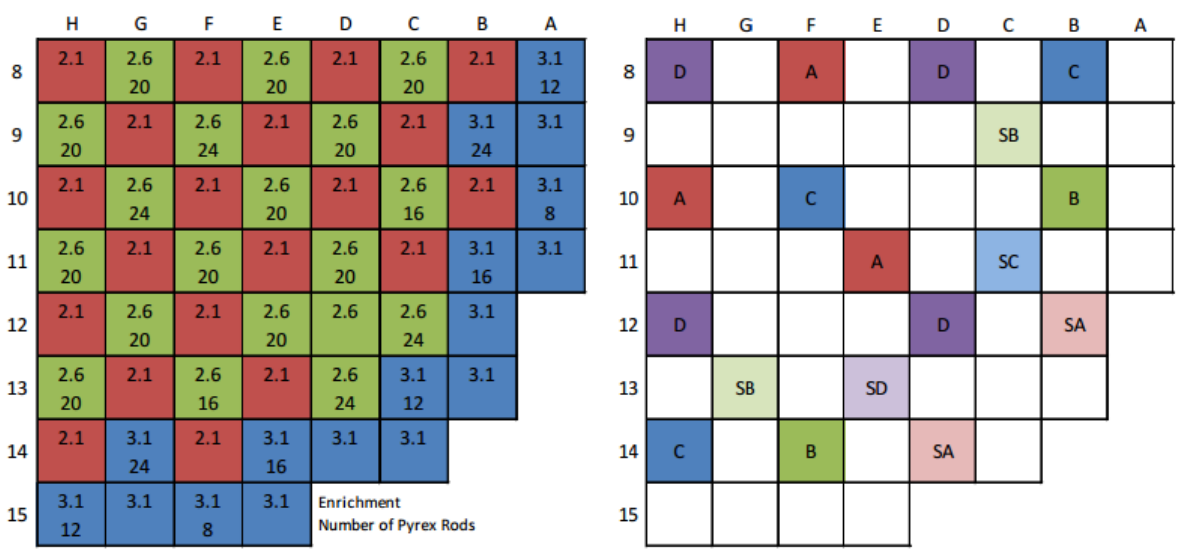

Figure 27: VERA Problem 5 Assembly, Poison, and Control Rod Layout in Quarter Symmetry

A full description of the problem is presented in "VERA Core Physics Benchmark Progression Problem Specifications". As part of the MPACT validation, the VERA benchmark Problems 9 and 10 were performed which required the depletion of the first cycle of Watts Bar Unit 1. The

following results were taken from the CASL report describing the completion of Problem 10 [Kochunas, 2014]. One of the principal features in Problem 10 was the requirement to shuffle the fuel from Cycle 1 into the Cycle 2 loading pattern as shown in Figure 28. The purple assemblies describe the fresh feed assemblies being added, along with what IFBA and WABA loading are present. All other assemblies reference their previous x and y label location in cycle 1.

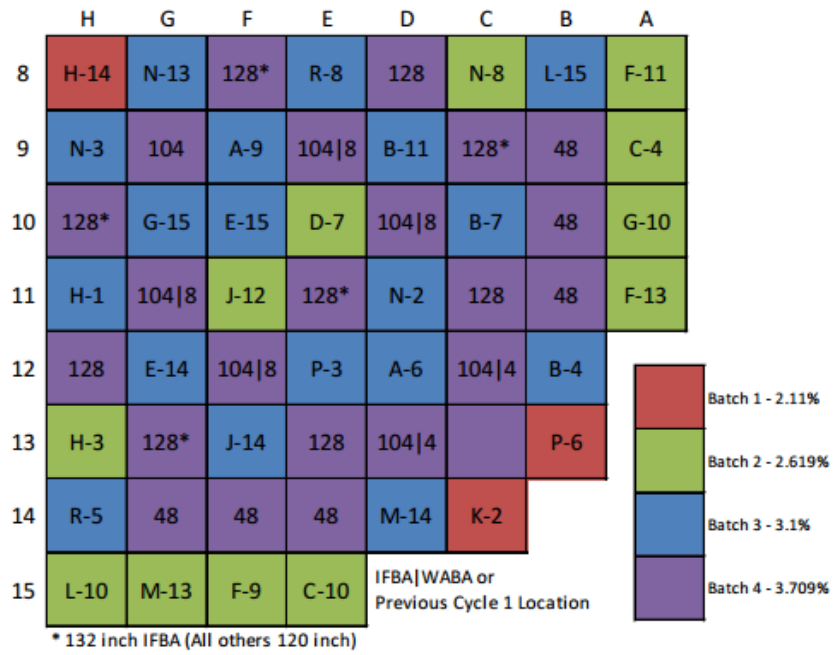

Figure 28: Problem 10 WBN1 Cycle 2 Core Loading Pattern

The cycle 1 operation history used to deplete cycle is shown in Table 13. The approximations include constant power over the cycle except for ramp-up and coast-down and constant rod position. The MOC discretization and the Chebyshev-Gauss quadrature was used with 16 azimuthal angles per octant and 4 polar angles per octant and a ray spacing of 0.05 cm. Transport corrected P0 based on the neutron leakage conservation with the out-scatter approximation was used for the scattering treatment. The standard 47 group MPACT library was used with the internal ORIGEN-based depletion capability in MPACT since at the time of this result the ORIGEN-API was only available with a 56-group structure.

For thermal-hydraulics feedback, the coupling to CTF was used in which the direct-moderator heating fraction was set to 2% and the heat transfer coefficient for the fuel-clad gap was set to be 10,000 W/m^2-K which was obtained from a parametric study to achieve a target fuel temperature of 835 K in a pin cell calculation. The simulation was performed on the EOS compute cluster and the problem was decomposed in MPACT with 2378 spatial domains (58 axial and 41 radial) and 2 hyper-threads for a total of 4756 processors.

Table 13: Cycle 1 Simulated Operating History

State Index	Exposure (EFPD)	Power (%)	Bank D Position
1	0	1.00E-06	219
2	9	65.7	219
3	32	99.7	219
4	45	97.7	219
5	60	97.7	219
6	80	97.7	219
7	100	97.7	219
8	120	97.7	219
9	160	97.7	219
10	200	97.7	219
11	240	97.7	219
12	280	97.7	219
13	320	97.7	219
14	360	97.7	219
15	398.6	97.7	219
16	410.7	89.9	219
17	423.6	78.8	219
18	441	64.5	219

Results

The beginning of cycle power distributions are shown in Figure 29 for the HZP and HFP core conditions. The depletion results are shown in Table 12 and Figure 30. As indicated, the critical boron concentration generally is within 50 ppmB of measurement as noted by the black dashed lines in Figure 26. The in-core detector responses were calculated with MPACT, but the data was not available at the time the CASL-U-2014-0189-000 document was prepared. However, the objective of this milestone was primarily to demonstrate code functionality and not code accuracy. The demonstration of MPACT accuracy is an objective of a June 30, 2015 milestone L1.CASL.P11.02 [Godfrey, 2015] to "Qualify VERA-CS for multi-cycle PWR simulation capability". This milestone will use VERA-CS to model WBN1 Cycles 1-12 using TVA plant data (startup tests, critical borons, flux maps, etc) and actual fuel assembly design data provided by Westinghouse. For these calculations MPACT will be coupled to COBRA-TF for thermal-hydraulics and to ORIGEN for depletion and decay. Also an improved fuel temperature model based on BISON-CASL will be used together with an improved 47g sub-group cross sections. For this milestone, the MPACT results will be compared to continuous energy Monte Carlo (SHIFT) at various points in the burnup cycle. Detailed results will be provided for criticality, rod worths, temperature coefficients, boron concentrations, and flux maps to measured data. The results of this milestone will provide a substantial validation base for MPACT and will be included in the first revision of this document.

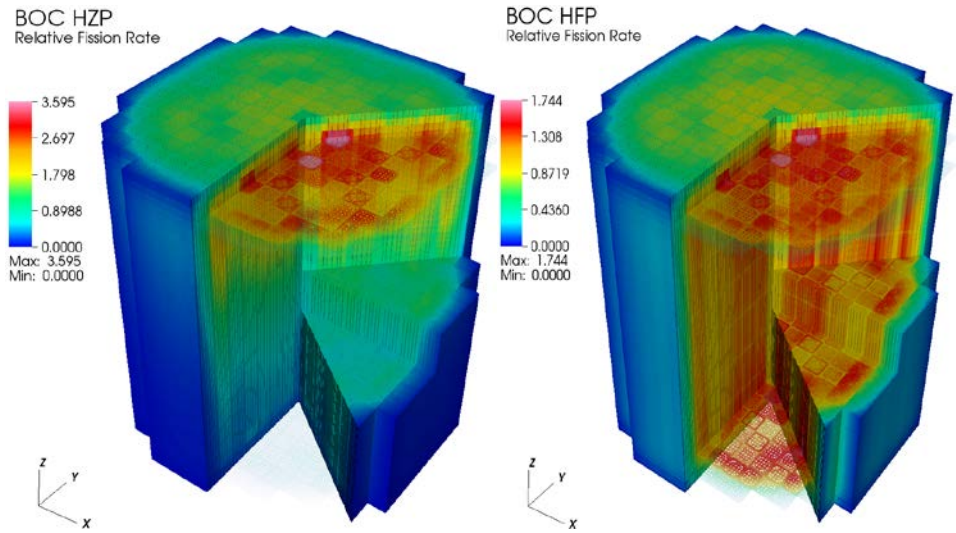

Figure 29: Core Power Distribution at BOC HZP (Left) and BOC HFP (Right)

Table 14: Measured and Simulated Cycle 1 States

Simulated						Measured			
Exposure (EFPD)	**Power (%)**	**Bank D**	**Boron (ppmB)**	**keff**	**Fuel Temp (K)**	**Exposure (EFPD)**	**Power (%)**	**Bank D**	**Boron (ppmB)**
0	1.0E-06	219	1909.54	1.00000	291.7	**0**	0		1299
9	65.7	219	1057.87	1.00000	756.9	---	---	---	---
32	99.7	219	841.79	1.00000	873.4	**32**	99.7	219	858
45	97.7	219	825.59	1.00000	866.0	**42.8**	100	215	848
60	97.7	219	816.29	1.00000	865.8	**55.9**	99.9	214	839
80	97.7	219	793.05	0.99999	865.3	**78**	99.9	208	823
100	97.7	219	762.39	1.00000	864.8	**105.8**	99.8	217	790
120	97.7	219	727.34	1.00000	864.4	**119.4**	99.8	212	763
160	97.7	219	646.76	1.00000	863.6	**156.4**	99.9	218	700
200	97.7	219	556.52	0.99999	862.8	**194.3**	98.9	215	592
240	97.7	219	455.65	1.00000	862.1	**249.6**	99.9	216	458
280	97.7	219	346.24	1.00000	861.4	**284**	99.9	218	363
320	97.7	219	229.35	1.00000	860.9	**314.5**	99.5	214	266
360	97.7	219	107.17	1.00000	860.5	**367.7**	100	216	111
398.6	97.7	219	1.0E-07	0.99873	860.1	**401.4**	99.6	217	7
410.7	89.9	219	1.0E-07	0.99720	833.3	**410.7**	89.9	216	9
423.6	78.8	219	1.0E-07	0.99667	796.0	**418.8**	83.4	228	9
441	64.5	219	1.0E-07	0.99564	750.0	**439.5**	65.3	227	9

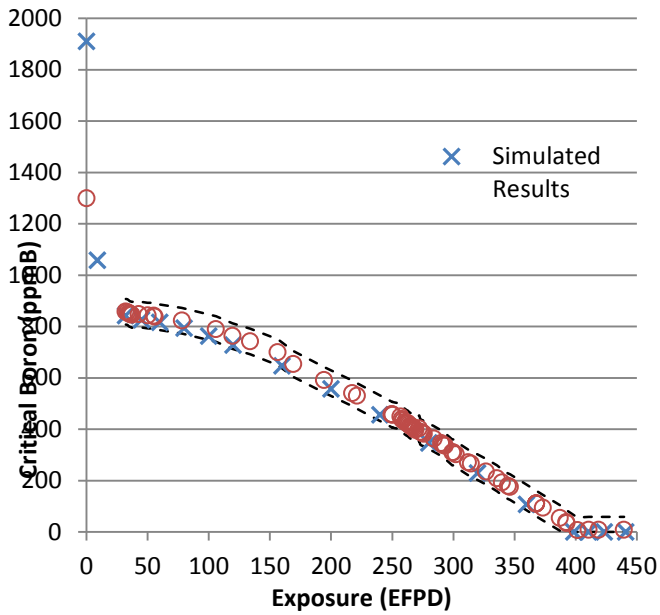

Figure 30: Comparison of Cycle 1 Critical Boron

3.2.2.2 BEAVRS

The Benchmark for Evaluation And Validation of Reactor Simulations (BEAVRS) is a publicly available reactor specification provided by the Massachusetts Institute of Technology (MIT) Computational Reactor Physics Group [Horelik, 2013]. The three region core loading and fuel enrichments are also similar to WBN1 however there are some differences in the lattice pattern and discrete burnable absorber types than WBN1 The benchmark contains two cycles of detailed geometry and measurements from an unnamed utility's PWR, however, the BEAVRS reactor is a traditional Westinghouse 4-loop PWR very similar to WBN1. The measured data provided for BEAVRS includes Cycles 1 and 2 ZPPT results, power escalation and HFP measured flux maps, and HFP critical boron concentration measurements for both cycles. The power history for each cycle is provided, but the regulating bank history is not. The flux map data provided is the processed 61 level data.

Because BEAVRS is a public release from an unnamed utility, its data is limited and support is not readily available for problems or questions. Also, it is unlikely to be continued to any more cycles, which limits the long term value that could be gained (as opposed to benchmarking against a plant that is still operating, in cooperation with an end user). Nevertheless, this benchmark is becoming an industry standard for validation of advanced codes and a PHI milestone is being performed to validate MPACT using BEAVRS [Collins, 2015b].

3.2.2.3 KRSKO

The Krško Nuclear Power Plant is a Westinghouse 2-loop PWR operated by Nuklearna Elektrarna Krško (NEK) in Slovenia. Currently a Joint Development Project exists between Westinghouse and the Slovenian Jožef Stefan Institute (JSI) to analyze the measured plant data from Krško with the latest M&S tools, including VERA-CS. This effort is primarily being led by Westinghouse

[Franschesini, 2014]. Krško is very similar to the Point Beach and Prairie Island reactors in the U.S except for the fuel assembly design used (14x14). Krško began commercial operation in 1983 and consists of 121 fuel assemblies based on the Westinghouse 16x16 fuel lattice design. The fuel assembly composition is very similar to the 17x17 fuel, except the spacer grids are made of Inconel with type 304 stainless steel sleeves. The presence of moderate neutron absorbers in Inconel and stainless steel leads to a larger flux depression in grid locations compared to Zr-based grids. The clad is Zircaloy-4 with an outside diameter (OD) of 0.374 in, and a pellet OD of 0.3225 in; the fuel pitch is 0.485 in. This results in an H/U of ~3.6 and to a lower moderated lattice than other typical designs, e.g. ~ 4.0 for Westinghouse standard 17x17 fuel. The use of Krško for validation of MPACT will be an important contribution in terms of application of the code by Westinghouse, significant data availability, and mutually beneficial collaboration with engineers outside of CASL on a non-U.S. reactor.

3.3 Post Irradiation Examination / Depletion

The purpose of this portion of the validation plan proposed in [Godfrey, 2014] is to demonstrate the accuracy of the isotopic depletion and decay calculations in VERA-CS using whole core calculations as much as possible. The reactivity effects of depletion are also addressed by the power plant benchmarks but these only indirectly support the isotopic concentrations of the fuel, particularly those with large neutron cross sections. As noted [Godfrey, 2014] MPACT will enable more detailed comparisons to measured data than are typically performed due to the capability to explicitly model 3D pin-wise-powers, isotopic depletion, and decay. Such comparisons include the traditional radiochemical assay characterizations used to benchmark pin cell depletions or lattice physics codes, but also include axial gamma scans, radial pellet gamma scans, and inferred burnup distributions. The goal of this portion of the validation is to perform these calculations with as much reactor benchmarking data as possible for a fully integrated application of VERA-CS.

3.4 Continuous Energy Monte Carlo Benchmarks

This portion of the validation plan uses high-fidelity reactor simulations to augment the measured data discussed in the previous three sections. The use of continuous energy (CE) cross sections and Monte Carlo physics for particle transport represents the highest level of accuracy achievable by modeling and simulation tools and has become increasingly more prominent because of faster computers and more efficient parallel algorithms, as well as improved methods for Doppler broadening and thermal scattering interpolation. For the purposes of MPACT validation, Monte Carlo tools are being used for two main purposes.

First, Monte Carlo has been used extensively during the MPACT development process to model fuel pins, assemblies, and assembly cluster in both 2-D and 3-D. Specifically, the sequence of VERA benchmarks 1-4 involved various reactor problems for which critical experiments could not be performed but for which “benchmark quality” results were necessary to guide the development.

Second, Monte Carlo transport solutions are being used to provide reference to supplement critical experiment measured data. This was the case of the SPERT critical experiments which were presented in Section 3.2.

It is anticipated in the future, Monte Carlo benchmarks will play an increasingly important role, especially for multi-physics problems for which costly experiments may not be possible.

4 SUMMARY, CONCLUSIONS, FUTURE WORK

The objective of this document was to summarize the current state of MPACT V&V and to begin to establish the framework for future MPACT V&V activities. An overview was provided of the verification and validation process in MPACT, as well as a summary of the status of each component of V&V in the code.

During Phase I of CASL MPACT verification activities in the areas of source code verification have matured and an initial investigation was performed on the Method of Manufactured Solutions (MMS) to establish a more robust solution verification. During Phase II, several specific tasks are necessary to improve MPACT verification:

1. A concerted effort should be performed to improve the unit test coverage in MPACT. Currently there are some important functions that have very poor test coverage, and even though the overall coverage code coverage is about 80%, the current MPACT_Drivers coverage of 67% needs to be increased. A reasonable goal is for MPACT unit test coverage to be sustained at 90%.

2. The development of a plan to document all of the unit and regression tests in a consistent format that can be assimilated into a common document. One option is to build a latex template that can exist in the test directory which could include images of the geometry, what is tested, the pedigree of the reference solutions, known deficiencies, etc. This process could also serve as a whole code review and would require substantial effort. However, once established this would provide the centerpiece of MPACT verification.

3. The development of a plan for implementation of the Method of Manufactured Solution which will include the scope of the effort, as well as the manpower necessary to develop a fully automated tool.

4. The development of coordinated plan by UM and ORNL to define coding standards, code design standards, and standardize the workflow for joint development (e.g. the use of feature branches, prepush testing, etc.).

In the area of validation, work has been ongoing during Phase I in 3 out of the 4 of the principal areas identified by [Godfrey, 2014] in the VERA-CS validation plan. Specifically work has been and is being performed in items 1, 2, and 4 of the following:

1. Measured data from experiments with small critical nuclear reactors.
2. Measured data from operating nuclear power plants.
3. Measured isotopics in fuel after being irradiated in a nuclear power plant.
4. Calculated quantities on fine scales from continuous energy (CE) Monte Carlo methods.

The principal area that is not receiving sufficient attention is item 3, comparison of MPACT depletion results to measured isotopics in irradiated fuel. The current results on full core depletion are providing partial coverage of this area, but a focused effort on detailed isotopic distributions should be a priority in Phase II

Other Phase II activities which are important for MPACT validation would include the implementation of uncertainty quantification protocol, validation problems for pin resolved reaction rates, and insuring that the validation needs identified by the PCCM on the CASL challenge problems are covered by the MPACT validation suite. These are briefly discussed below.

Uncertainty Quantification Methods

As noted in [Oberkampf, 2008], the quantification of uncertainty in both the measured and the computed quantities is a central part of the code validation process. Without this information it is it is much more difficult to determine whether an MPACT result "passes" a particular benchmark when its results are compared to the measured data. While MPACT has been maturing as a neutronics code during Phase I of CASL, it has not been possible to formally implement UQ methods. However, the code appears to be sufficiently mature now to accommodate UQ so that this should be a top priority during Phase II.

Pin resolved validation

One of the principal distinguishing capabilities of the MPACT code is its ability to provide "pin resolved" neutron fluxes and powers during full 3D core calculations. This capability will support specific challenge problems within CASL such as the Pellet Clad Interaction. There is limited experimental data for validation of pin resolved reactor calculations. One of the principal efforts were the measurements performed at Paul Scherrer Institute in Switzerland from 2000-2007. In the context of the LWR-PROTEUS effort at PSI, measurements were made on the radial and azimuthal U235 fission and U238 capture distributions in BWR UO2 pins [Macku, 2007]. Supporting calculations were performed with both the deterministic code CASMO-4 and the continuous Monte Carlo code MCNP4 and compared with activation foil measurements. Reaction rate distributions were calculated for zero-burnup pins of a Westinghouse SVEA-96 Optima2 boiling water reactor fuel assembly as shown in Figure 31 which was taken from the paper.

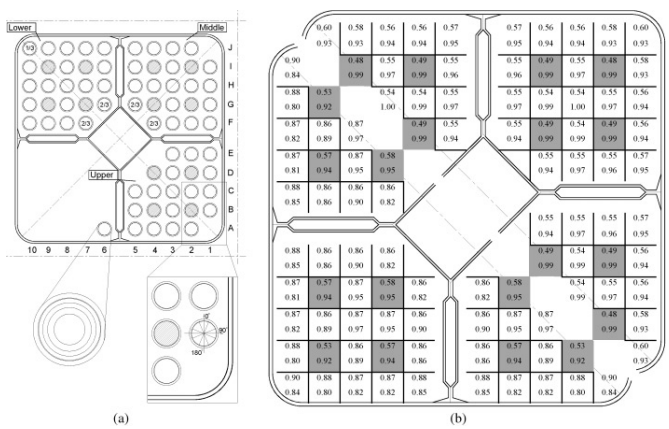

Figure 31: Westinghouse Optima2 Fuel Assembly Used for Pin Measurements [Macku, 2007]

The within-pin distributions predicted by the two codes were in good agreement for some pins however there were significant discrepancies in the U238 capture predictions between the codes for the peripheral pin in the southwest quadrant, both azimuthally and radially. The MCNP4C within-pin distributions were much more accurate than those of CASMO-4 which showed discrepancies of as much as 8% in some locations compared to measurements. During Phase II, the use of data such as the pin resolved measurements at PSI should be included in the MPACT validation effort.

MPACT Validation for Challenge Problems

The MPACT validation effort described in this document did not explicitly consider those phenomena which might play a significant role in the CASL challenge problems. A separate activity is being led by the VMA focus area to perform Predictive Code Maturity Model (PCMM) evaluation for each of the challenge problems. A preliminary analysis was performed [Mousseau, 2014] for CIPS, PCI, and DNB, and determined that the following is a list of important phenomenon for MPACT.

1. Energy deposition
2. Fast flux
3. Isotopics
4. Gamma heating
5. Fission power
6. Fission product yield
7. Cross sections
8. Boron feedback to neutronics
9. Decay heat model (retards cool-down)
10. Burn up

In general, most of these phenomena will be covered in the course of the normal MPACT validation. However, the VMA list should be explicitly taken into consideration when prioritizing future MPACT validation exercises.

Summary

During Phase I of CASL MPACT verification activities in the areas of source code and verification have matured and a plan is being established to provide a more robust solution verification effort based on the Method of Manufactured Solutions. In the area of validation, work has been ongoing during Phase I in both areas of measured data from experiments with small critical nuclear reactors, as well as measured data from operating nuclear power plants. Both of these areas have been supplemented with calculated quantities on fine scales from continuous energy (CE) Monte Carlo methods. Based on the results of Phase I V&V, the confidence level has increased in the ability of MPACT to model an operational Pressurized Water Reactor and a roadmap has been established by the VERA-CS Validation Plan to guide the efforts during Phase II and to further increase the validation base of the code.

Several specific tasks have identified to improve MPACT verification during Phase II of CASL, to include a task to improve the unit and regression test coverage in MPACT, a task to develop a plan to document all of the unit and regression tests in a consistent format that can be assimilated into a common document, and a joint UM/ORNL task to develop standardize coding standards and workflow for the continued collaborative development of MPACT.

Several specific tasks were identified to improve MPACT validation during Phase II such as depletion validation with measured isotopics, the implementation of a formal data uncertainty quantification (UQ) protocol in MPACT, the addition of problems to validate the pin resolved capability in MPACT, and a coordinated effort with VMA to insure that the validation needs identified by the PCCM on the CASL challenge problems are covered by the MPACT validation suite.

REFERENCES

[Seiger, 2015] M. Seiger, CASL-QA-030, CASL Software Quality Assurance Requirements, January, 2015, CASL-U-2015-0010-000

Oberkampf, W. L., S. M. DeLand, B. M. Rutherford, K. V. Diegert and K. F. Alvin (2002), "Error and Uncertainty in Modeling and Simulation," Reliability Engineering and System Safety, Vol. 75, No. 3, 333-357.

Oberkampf, W. L. and T. G. Trucano (2002), "Verification and Validation in Computational Fluid Dynamics," Progress in Aerospace Sciences, Vol. 38, No. 3, 209-272.

Oberkampf, W. L., T. G. Trucano, and C. Hirsch (2004), "Verification, Validation, and Predictive Capability," to appear in ASME Applied Mechanics Reviews, (also SAND-2003-3769).

Oberkampf, W. L. and M. F. Barone (2004), "Measures of Agreement Between Computation and Experiment: Validation Metrics," 34th AIAA Fluid Dynamics Conference, AIAA Paper No. 2004-226, Portland, OR.

[Kolowa, 2007] Kolawa, Adam (2009-07-01). "Unit Testing Best Practices". Retrieved 2012-07-23.

[Collins, 2015] B. Collins, ORNL, Expand Capability and Coverage of MPACT Regression Test Harness, RTM Milestone, L3RTM.PRT.P10.04, 2015.

[Wang, 2014] "Sensitivity Study of MOC Parameters with VERA Benchmark Cases", Jipu Wang, Department of Nuclear Engineering and Radiological Sciences, University of Michigan, December 2014

[Pautz, 2001] Shawn D. Pautz, 2001, Verification of Transport Codes by the Method of Manufactured Solutions: The ATTILA Experience, LA-UR-01-1487

[Roache, 2002] Code Verification by the Method of Manufactured Solutions, Journal of Fluids Engineering, MARCH 2002, Vol. 124, pp 4-10.

[Baldwin, 1979] Baldwin, M. N., et al., Critical Experiments Supporting Close Proximity Water Storage of Power Reactor Fuel, B&W-1484-7, Babcock & Wilcox, July 1979.

[Newman, 1984] Newman, L.W., Urania-Gadolinia: Nuclear Model Development and Critical Experiment Benchmark, DOE/ET/34212-41, B&W-1810, Babcock & Wilcox, April 1984

[Kulesza, 2015] J. Kulesza, S. Stimpson, A. Gerlach, D. Jabaay, CASL-X-201X-0XXX-000 Babcock and Wilcox Critical Experiment Calculations to Support MPACT Validation, April 24, 2015.

[Herman, 2013] B. R. Herman, B. Forget, and K. Smith, "Improved Diffusion Coefficients Generated from Monte Carlo Codes," in Proceedings of the M&C 2013 ANS Meeting, (LaGrange Park, IL, USA), American Nuclear Society, 2009.

[Bowman, 2011] Bowman, S. M., 2011. SCALE 6: Comprehensive Nuclear Safety Analysis Code System, Nucl. Technol. 174(2), 126-148.

[Durgone, 1965] Durgone, J., 1965. SPERT III Reactor Facility: E-CORE Revision, p. 18, AEC Research and Development Report IDO-17036.

[Kochunas, 2014] B. Kochunas, et al., "Operational Reactor Depletion Capability," CASL-U-2014-0189-000, September 30, 2014.

[Franceshini, 2014] Franceschini, F. and A. T. Godfrey, Benchmark of VERA Depletion and Comparison with Industry Code, CASL-I-2014-0195-000, CASL, September 2014.

Horelik, H., et at., Benchmark for Evaluation and Validation of Reactor Simulations (BEAVRS), Release Revision 1.1.1, MIT Computational Reactor Physics Group, October 2013.

[Collins, 2015b] B. Collins and A. Godfrey, "Analysis of BEAVRS Benchmark Using MPACT," ANS M&C 2015, Nashville, TN, April, 2015.

[Macku, 2007] K. Macku, et al., "Radial and azimuthal U235 fission and U238 capture distributions in BWR UO2 pins: CASMO-4 and MCNP4 versus activation foil measurements, NSE, 155, 96-101.

[Mousseau, 2014] V. Mousseau, N. Dinh, Y. Sung, J. Secker, R. Montgomery, "CASL Code Validation Plans," December, 2014.

[Oberkampf, 2008] William L. Oberkampf, Timothy G. Trucano Verification and validation benchmarks *Nuclear Engineering and Design, Volume 238, Issue 3, March 2008, Pages 716-743*

[Godfrey, 2015] "Qualify VERA-CS for Multi-cycle PWR simulation capability", L1.CASL.P11.02, June 30, 2015.